

# SOLID FRICTION FROM STICK-SLIP DOWN TO PINNING AND AGING

Tristan Baumberger, Christiane Caroli

*Institut des Nanosciences de Paris [†], 140 rue de Lourmel, 75015 Paris (France)*

(Dated: October 29, 2018)

We review the present state of understanding of solid friction at low velocities and for systems with negligibly small wear effects.

We first analyze in detail the behavior of friction at interfaces between macroscopic hard rough solids, whose main dynamical features are well described by the Rice-Ruina rate and state dependent constitutive law. We show that it results from two combined effects : (i) the threshold rheology of nanometer-thick junctions jammed under confinement into a soft glassy structure (ii) geometric aging, *i.e.* slow growth of the real area of contact via asperity creep interrupted by sliding.

Closer analysis leads to identifying a second aging-rejuvenation process, at work within the junctions themselves. We compare the effects of structural aging at such multicontact, very highly confined, interfaces with those met under different confinement levels, namely boundary lubricated contacts and extended adhesive interfaces involving soft materials (hydrogels, elastomers). This leads us to propose a classification of frictional junctions in terms of the relative importance of jamming and adsorption-induced metastability.

## I. INTRODUCTION

### A. From Amontons-Coulomb to Rate-and-State

For more than two centuries, the description of solid friction commonly used in mechanical modelling was provided by the classical Amontons-Coulomb laws. They state that, when a nominally planar solid block lying on top of a planar track is submitted to a normal force  $W$  and a tangential one  $F$  (Figure 1) :

- No motion occurs as long as  $F$  is smaller than a finite threshold  $F_s$ .

- Sliding is dissipative, and the corresponding dynamical friction force  $F_d$  is constant and equal to  $F_s$ .

- Their common value  $F$  is proportional to the normal load  $W$  and, for a given  $W$ , independent of the macroscopic contact area  $\Sigma$ . Hence, the frictional behavior of a couple of materials is characterized by a single *number*, the friction coefficient :

$$\mu = \frac{F}{W} \quad (1)$$

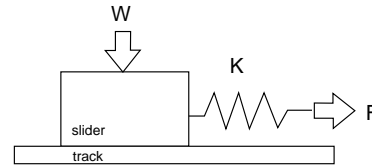


FIG. 1: A schematic slider-on-track system : the slider is pressed onto the track by the normal force  $W$ , and pulled by the tangential force  $F$  imposed through a driving stage of stiffness  $K$ .

An established tradition, when writing about solid friction, is to date its emergence as a well identified scientific question from Leonardo da Vinci (*ca* 1500). This makes it an unusually longstanding problem, since both its fundamental physical aspects and its modelization for the purpose of studies of *e.g.* seismic fault dynamics are still under lively debate nowadays (see for example [1], [2], [3], [4]). A very important progress in its phenomenologic modelling, for macroscopic solids, was accomplished with the formulation of the so-called *rate and state constitutive laws*, which emerged in the 70's from the work on rock friction of Dieterich [5], Rice and Ruina [6].

It was later shown that, inspite of their simplicity in terms of number of parameters, they provide an excellent description of most of the salient features of the low-velocity frictional dynamics of a wide variety of materials, ranging from granite to paper. Such an amazing “universality” is naturally appealing for the physicist, since it suggests :

- The possibility of a unified, largely material-independent, description on the underlying microscopic level.

- One step further, a possible feedback in terms of limitations and/or refinement of the mechanical constitutive laws.

It is on this particular approach, deliberately different from that of tribology proper <sup>1</sup>, but which parallels those presently developed in the fields of plasticity of amorphous materials [7] and rheology of jammed systems [8], that we concentrate here.

<sup>1</sup> This means, in particular, that we limit ourselves to systems and sliding regimes such that wear and frictional self-heating play a negligible role.

(threshold plus constant yield stress), and thus probably carries unphysical singularities as is the case of the Hill model.

Indeed, various departures from this description or its implications have gradually emerged, the most salient of which are the following :

(i) In general, the static friction coefficient  $\mu_s$  is larger than the dynamic one  $\mu_d$ .

(ii)  $\mu_s$  is not a mere number, but a slowly *increasing* function of the so-called *waiting time*  $t_w$ , i.e. the duration of static contact prior to sliding.

(iii) When measured in *stationary sliding*,  $\mu_d$  is not constant. In particular, for low enough velocities (typically  $< 100 \mu\text{m}\cdot\text{sec}^{-1}$ ) it is a slowly *decreasing* function of  $V$ .

That a stationary  $\mu_d$  can be measured is then by itself a puzzle, since such a velocity-weakening characteristic is well known to make steady motion always unstable : a positive (negative) velocity fluctuation induces a decrease (increase) of the friction force, leading to further acceleration (deceleration), thereby getting amplified. Indeed, when a slider is pulled at a low enough velocity through a driving stage, necessarily of finite stiffness, non steady sliding is frequently observed : the motion is jerky, alternating between “stick” periods of rest during which the stage stores elastic energy, and slip events (Figure 2). However, as skilled mechanical engineers have known already for long, these stick-slip oscillations disappear upon stiffening the driving stage, and steady sliding is realized.

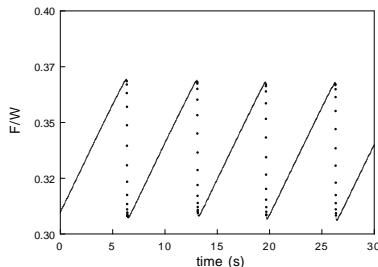


FIG. 2: Reduced tangential force *vs* time in the stick-slip regime for a paper/paper interface. From ref.[9].

This paradox points towards some inadequacy in the implicit assumption underlying the above instability argument - namely that the stationary  $\mu_d(V)$  function can be used as such to describe non steady motion. In other words, one suspects that the dynamic friction force does not only depends on the *rate variable*, i.e. the instantaneous sliding velocity.

(iv) Non steady friction is hysteretic, as illustrated on Figure 3, which shows the instantaneous friction force associated with a velocity cycle for which inertia is negligible.

(v) Dieterich [5] has studied the frictional response to a sudden jump of the driving velocity from  $V_i$  to  $V_f$  (Figure 4). He showed that it exhibits a transient the span

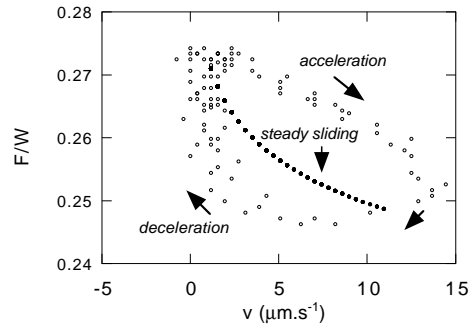


FIG. 3: Hysteretic friction force response of a paper/paper system in non-steady sliding (open circles) and for steady sliding at various velocities  $V$  (full circles).

of which is controlled by a characteristic *length*  $D_0$ , of micrometric order. That is, its duration  $\Delta t \approx D_0/V_f$ .

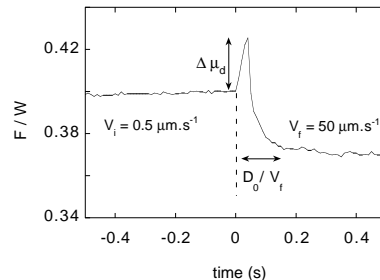


FIG. 4: Friction force transient following a jump of the driving velocity at  $t = 0$  from  $V_i$  to  $V_f$ , for a PMMA/PMMA interface. (Courtesy of L. Bureau)

These observations can be translated into the following statements :

- A frictional interface at rest becomes stronger as time lapses : it strengthens when *aging* (see (ii)).
- When sliding, it becomes weaker (see (i)) : it can be said to *rejuvenate upon sliding*. Moreover, its dynamic age in steady motion decreases with increasing  $V$  (see (iii)).
- This, together with (iv) and (v), means that its physical *state* evolves with a dynamics characterized by the length  $D_0$  and coupled to the sliding dynamics itself.

Rate and state constitutive laws model such behaviors in terms of a single (or a few) dynamical *state variable(s)*, the physical nature of which often remains unspecified. In such a situation, the physicist’s approach aims at identifying the physical content embedded in the state variables, and at justifying on this basis their phenomenological dynamics. One may then hope, as a side benefit of importance, to be able to predict their limits of validity and, possibly, to propose some further extensions.

## B. Spatial scales

For this purpose, a natural first step is to identify the relevant length scales. In the case of friction between macroscopic solids, this immediately leads to distinguishing between two classes of systems.

(A) **Rough hard solids** for which “reasonable” loading levels (apparent pressures  $W/\Sigma$  well below elastic moduli) do not result in an intimate molecular contact along the whole interfacial area.

For them a first relevant length scale is the average size of the *microcontacts* – the spots which form the real area of contact  $\Sigma_r$ . It lies usually in the *micrometric* range. Moreover, we will see that a detailed analysis leads to attributing ultimately frictional dissipation to *elementary mechanical instabilities* involving molecular rearrangements on the *nanometric* scale.

(B) **Soft and/or smooth solids** which are able to get into intimate contact everywhere along their interface. For them, the *nanometric* scale retains its importance, while the mesoscopic one becomes irrelevant.

In both cases, due to the long range of elastic interactions, a third important length scale is the *global size of the system*  $L$ . Its value has a crucial bearing on the spatial (in)homogeneity of the frictional motion, hence on the complexity of the sliding dynamics.

An important consequence, not to be overlooked, results straightforwardly from the identification of these spatial scales. Reducing the “state” of the interface to one or a few variables necessarily implies a statistical averaging, which can be meaningful only if performed on a large number of units. This entails that a rate and state phenomenology of friction is legitimate only on scales larger than a finite cutoff. In particular, when using discretized (block) models for e.g. numerical studies of extended interface dynamics, the basic block size must remain much larger than either the average intercontact distance (class (A)) or at least the ultimate nanometric scale (class (B)). That is, we contend that the question of the regularity of the continuum limit of discretized models — a subject of debate in the field of mode II interfacial fracture along seismic faults [10] — though of course mathematically sound, is physically irrelevant : if it should turn out that a continuum description of the fracture head zone would imply lengths smaller than the intercontact distance, the interface could no longer be assumed to have homogeneous frictional properties, but should be explicitly treated as a juxtaposition of frictional (contact) and non-frictional (non-contact) regions.

## C. Outline

Following Tabor [11], it is both useful and physically sound to express the friction force between two solids as

$$F = \sigma_s \cdot \Sigma_r \quad (2)$$

where  $\Sigma_r$  is the real contact area, and the stress  $\sigma_s$  is the so-called shear strength of the interface.

Section II is devoted to friction at multicontact interfaces between rough hard materials (MCI), an interfacial configuration which is prevalent when dealing with macroscopic bodies. We first analyze their geometry, then show that the geometric factor  $\Sigma_r$  plays, for these systems, the part of a state-dependent variable, governed by what we will call the *geometric age*  $\phi$ . We then show that, for MCI, the rate dependence of the rheological factor  $\sigma_s$  can be assigned to local mechanical instabilities within the nanometer-thick molecular “junctions” forming the real contacts. On this basis, the Rice-Ruina constitutive law, which they originally formulated on a phenomenological basis, results as a good approximation for the low velocity frictional behavior of MCI. We sketch out its consequences in terms of the sliding dynamics of a driven spring-block system. We also point out its various limits of validity.

These limits turn out to be of two different types.

- On the one hand, within the physical framework which identifies “state” with geometric age, the phenomenological functional expression of  $\Sigma_r(\phi)$  is necessarily approximate, and its limits can be evaluated.

- On the other hand, the detailed analysis of experiments brings to light the limits of the above physical framework itself. That is, it prompts the idea that a second underlying slow dynamics manifests itself through the rheological factor : *geometric age is not the whole story, frictional contacts also have a structural age.*

This leads us to concentrate, in Section III, on the rheology of frictional contacts. We analyze it for various configurations (rough-on-flat MCI, surface force apparatus (SFA), extended soft contacts) corresponding to various confinement and compacity levels. In all cases, it appears that *structural aging/rejuvenation mechanisms are indeed at work in the contact-forming nanometer-thick interfacial junctions.* The associated dynamics is quite strongly system-dependent. As a guide for future investigation, we suggest a first level of classification which distinguishes between two main types of dissipative behaviors, namely :

- (i) jammed junction plasticity, akin to that of soft glassy materials;

- (ii) adsorption–desorption controlled dynamics.

MCI microcontacts belong to class (i), gel/glass contacts to class (ii). Both mechanisms probably contribute to friction in SFA contacts, while the case of elastomer/glass remains open to discussion.

## II. MULTICONTACT INTERFACES

The renewal of interest for solid friction in the past 20 years, triggered by the work of rock mechanicians, was aimed at modelling friction along seismic faults. For this reason, it naturally focussed on MCI. It has resulted in bringing to light robust features shared by a wide variety of materials. We will see that this has led to the building a complete framework of description, namely :

- a predictive constitutive law
- an underlying physical interpretation opening onto further questions concerning contact rheology (Section III).

This is why MCI friction is treated here extensively.

### A. Geometry of multicontact interfaces

#### 1. Surface roughness

Consider two macroscopic solids (Figure 1), referred to as slider and track, with nominally planar contact surfaces. Nominally means here that they are flat on large scales comparable with the macroscopic slider lateral size. It is well known that, due to the unavoidable presence of steps, atomic flatness cannot be realized over lengths much beyond the micrometric scale. An exception is provided by lamellar solids, in particular cleaved mica for which this range may reach up to  $\sim 1$  cm. Optically smooth surfaces, with r.m.s. roughness on the order of a few nanometers over  $1 \text{ cm}^2$ , are uncommon, examples being provided by float glass and some highly polished metals. In general, natural or ground surfaces exhibit a r.m.s. roughness between 0.1 and a few microns on  $1 \text{ cm}^2$ .

Such random surfaces exhibit asperities with distributed heights, so that physical contact between them occurs only at random spots, the *microcontacts* between load-bearing asperities. They form what we call multicontact interfaces (MCI) (Figure 5).

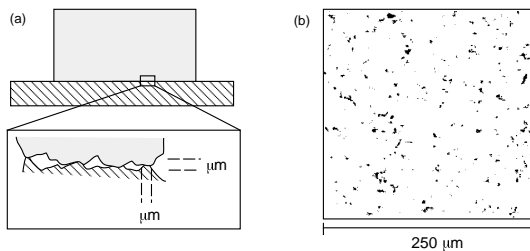


FIG. 5: (a) Schematic view of a multicontact interface between two nominally planar rough solids. (b) Optical visualization of the light-transmitting real contacts at the MCI between two transparent epoxy resin blocks. The contrast has been inverted. (Courtesy of O. Ronsin)

It is Tabor [11], in his pioneering work, who empha-

sized the importance of distinguishing between the apparent and the real areas of contact,  $\Sigma_{app}$  and  $\Sigma_r$ , and of evaluating the average microcontact size  $\bar{a}$ . It has emerged (see below) that typical values for  $\Sigma_r/\Sigma_{app}$  and  $\bar{a}$  are respectively  $10^{-3}$  and a few microns. This means that a typical MCI is formed of a sparse set of microcontacts with average separation  $\simeq 100 \mu\text{m}$  – a picture which has been confirmed by direct optical observation ([12] and Figure 5). It is intuitively clear that increasing the normal load  $W$  results in decreasing the distance between the average surface planes (the so-called “closure”), hence in increasing the number of microcontacts as well as the area of preexisting ones :  $\Sigma_r$  increases with  $W$ , as illustrated by Dieterich’s observations [12]. Can one make the functional nature of this dependence explicit? Does it depend on the statistical nature of the surface roughness and if so, how? Could it be that this dependence would explain the Amontons proportionality between  $F$  and  $W$ ?

#### 2. The single microcontact

As a first step, let us recall a few basic results from contact mechanics concerning a single contact. Let us focus on the a single pair of contacting asperities, modelled as elastic spherical caps with a common radius of curvature  $R$  and Young modulus  $E$ , pressed together by a normal force  $w$  acting along their intercenter axis. The problem of the resulting elastic contact was fully solved by Hertz and is equivalent to that between a rigid plane and an elastic sphere of radius  $R^* = R/2$  and Young modulus  $E^* = E/2(1 - \nu^2)$ , with  $\nu$  the Poisson modulus [13].

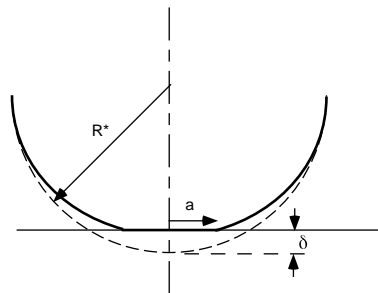


FIG. 6: Hertz contact between an elastic sphere and a rigid plane.

Its solution can be evaluated as follows. Due to the spherical geometry, the contact diameter  $a$ , the “compression”  $\delta$  (Figure 6) and  $R^*$  are related by  $a^2 \sim R^* \delta$ . As can be checked from the full Hertz solution [13], the elastic energy is essentially stored within a depth on the order of the contact radius, hence the relevant strain level  $\epsilon \sim \delta/a$ , so that the average normal stress  $\bar{p} \sim w/a^2 \sim E^* \epsilon \sim \delta/a$ . From this it immediately results that, dimensionally

$$a \sim \left(\frac{wR^*}{E^*}\right)^{1/3} \quad \delta \sim \left(\frac{w^2}{R^*E^{*2}}\right)^{1/3} \quad \bar{p} \sim \left(\frac{wE^{*2}}{R^{*2}}\right)^{1/3} \quad (3)$$

The exact expressions (see [13]) only differ by multiplicative constants of order unity.

Now, most solids are truly elastic only up to a yield stress  $Y$ , beyond which they start deforming plastically. So, the Hertz expressions above lose validity when the maximum normal stress below the contact reaches this level. Upon increasing the normal load, the size of the plastified region increases, until it occupies a volume  $\sim a^3$ . At this stage the contact has become “fully plastic” and deforms so that the normal stress remains quasi-constant :  $\bar{p} \simeq H$ , where  $H$  is the *hardness*<sup>2</sup> of the softer material. At room temperature, for metals, the ratio  $H/E$  ranges in general between  $10^{-2}$  and  $10^{-3}$ , while for polymer glasses,  $H/E \simeq 10^{-1} - 10^{-2}$ . Imagine now, following Bowden and Tabor [11], that the apparent pressure  $p_{app} = W/\Sigma_{app}$  is large enough for this regime to be reached in all the microcontacts forming a MCI. Then, the real area of contact is such that  $\Sigma_r/\Sigma_{app} \simeq p_{app}/H$ , and  $\Sigma_r \simeq W/H$ .

So, in the fully plastic regime,  $\Sigma_r$  is proportional to the normal load, and Amontons’s law simply follows. Indeed the friction coefficient reads :

$$\mu = \frac{F}{W} = \frac{\Sigma_r}{W} \simeq \frac{\sigma_s}{H} \quad (4)$$

Since, in this approximation,  $\sigma_s$  is the shear strength under the constant normal stress  $H$ ,  $\mu$  is effectively  $W$ -independent. However rough it is, this approximation is illuminating in several respects.

On the one hand, the a priori surprising fact that the values of dry friction coefficients depend only weakly on the mechanical properties of materials and are commonly a fraction of unity can now be translated into the statement : interfacial shear strength values are roughly comparable with bulk yield stress levels — a point which will be of qualitative importance later on.

On the other hand, it permits to get a somewhat more precise idea about the minimum loading level necessary to form a MCI between given materials. Consider as an example a 1 cm thick steel plate under its own weight. Then  $p_{app} \simeq 10^3$  Pa, while  $H \simeq 10^9$  Pa, hence  $\Sigma_r/\Sigma_{app} \simeq 10^{-6}$  : a 1 cm<sup>2</sup> surface would form no more than about 10 microcontacts of area  $10\mu\text{m}^2$  (see below) – hardly enough to form a decent statistical set!

Tabor’s suggestion, which he developed for the case of metals, later gave rise to a number of discussions about

the relevance of the full plasticity assumption to wider classes of materials which also obey Amontons’s law while being less ductile than metals. This opened onto the problem of modelling the elastic-plastic contact between random surfaces.

### 3. Area of contact between random surfaces

The crucial contribution to this question was made by Greenwood and Williamson [15]. Their model reduces the characterization of each of the contacting random surfaces to :

- the statistical distribution of asperity summit heights above some average plane  $\phi(z)$ . These asperities are assumed to have spherical tips.
- the asperity radius of curvature  $R$ , assumed to be unique.
- the number of summits  $N$  on the apparent surface  $\Sigma_{app}$ .

They show that the problem of contact between two such nominally flat elastic random surfaces can be cast into that of a “composite” random surface and a rigid plane [13].

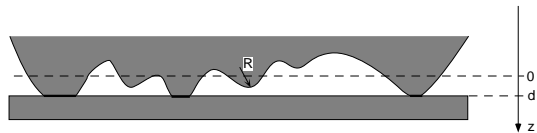


FIG. 7: Schematic representation of a Greenwood-Williamson interface (see text).

Let  $d$  be the separation between the average plane and the rigid one (Figure 7),  $n$  the number of microcontacts at this separation, assumed to be dilute enough to be treated as independent Hertz contacts. Each asperity with height  $z > d$  contributes to  $n$  :

$$n = N \int_d^\infty dz \phi(z) \quad (5)$$

The compression of a contact is  $(z-d)$ , its area  $\pi R(z-d)$ , and it bears the load  $(4/3)\pi R^{1/2}(z-d)^{3/2}$  (eq.(3), [13]) so that the real area of contact

$$\Sigma_r = N \int_d^\infty dz \pi R(z-d)\phi(z) \quad (6)$$

and  $d$  is related to the given total normal load  $W$  by :

<sup>2</sup> On the basis of geometric arguments, one estimates that  $H \simeq 3Y$ [14].

$$W = N \int_d^\infty dz (4/3)\pi R^{1/2}(z-d)^{3/2}\phi(z) \quad (7)$$

The main physical content of the Greenwood - Williamson (GW) results already emerges under the schematic assumption of an exponential distribution  $\phi_0(z) = s^{-1}\exp(-z/s)$  for  $z > 0$  and zero otherwise. One then gets :

$$n = \frac{1}{\sqrt{\pi}} \frac{W}{ER^{1/2}s^{3/2}} \quad \Sigma_r = \sqrt{\pi} \left(\frac{R}{s}\right)^{1/2} \frac{W}{E} \quad (8)$$

Both  $\Sigma_r$  and the number of contacts are proportional to  $W$ , and individual contact sizes grow under increasing load in such a way that the average contact radius :

$$\bar{a} = \left(\frac{\Sigma_r}{\pi n}\right)^{1/2} = \sqrt{Rs} \quad (9)$$

remains a load-independent constant.

GW have shown numerically that these properties are conserved, to a very good approximation, for a gaussian distribution of summit heights, in the load range, ranging over several decades, such that  $1 \ll n \ll N$ . A rough evaluation of  $N$  is obtained by representing  $\Sigma_{app}$  as densely paved by average asperities of curvature  $R^{-1}$  and height  $s$ , so that  $N \sim \Sigma_{app}/Rs$ . The upper limit then translates into

$$\frac{p_{app}}{E} \ll \sqrt{\frac{s}{R}} \quad \text{or} \quad \Sigma_r \ll \Sigma_{app} \quad (10)$$

Note that this condition also ensures that elastic interactions between microcontacts can reasonably be neglected.

A considerable amount of work [16] has been devoted to evaluating the two geometrical parameters involved in the GW model on the basis of surface topography measurements. Curvature determinations have been hotly debated, since they involve a second order derivative of the profile, which makes them strongly noise-sensitive. When measured with profilometers of lateral resolution of micrometric order, typical values of  $R$  for surfaces blasted or lapped with abrasive powders commonly lie in the 10 – 100 $\mu\text{m}$  range [17] [15] [18], while r.m.s. roughnesses  $s \sim 1\mu\text{m}$ . Then the corresponding average contact radii  $\bar{a} \sim 3 - 10\mu\text{m}$ , an estimate which has been confirmed from the Dieterich-Kilgore visualizations [12].

Modern experimental improvements have revealed that surface profiles are in general more complex than was initially assumed by GW, exhibiting multiscale roughness distributions [19]. They are often modelled as self-affine

surfaces<sup>3</sup>.

Persson [20] has recently proposed a theoretical treatment of the resulting contact problem. His calculation of the contact area between a flat compliant medium and a rigid self-affine surface follows a renormalization scheme for the stress distribution for profiles at growing stages of magnification  $\zeta$ . This function he proves to obey, for *complete* contact between the surfaces, a Fokker-Planck-like equation, with  $\zeta$  playing the part of time. The real case of incomplete contact is then simulated via a boundary condition eliminating from the area of contact the regions sustaining tensile stress. This enables him to express the solution in terms of the elastic response of the compliant medium to imposed displacements specified all along its surface — while partial contact actually corresponds to a mixed situation of given displacements within contacts and given (null) normal stress elsewhere. It is therefore difficult to assess the influence of the ansatz on the main result of interest here, namely that the real contact area still obeys the Amontons proportionality  $\Sigma_r \sim W$ .

Note that Persson's result depends crucially on the physical existence of a lower cut-off of the spatial scales, which is in practice of mesoscopic order. Indeed, even in the highly improbable case where the fresh surfaces would remain fractal down to the atomic scale, the nano-asperities would get plastified, and thus smoothed out, under the very high pressures they would experience upon contact.

This remark brings up the important question of the limit of validity of the pure elastic contact models. Clearly, when thinking in GW's terms, plastic deformation of asperities starts coming into play when the average pressure  $\bar{p}$  becomes comparable with the yield stress  $Y$ . From equations (8) and (9), this condition can be expressed in terms of the dimensionless plasticity index

$$\psi = \frac{E}{Y} \sqrt{\frac{s}{R}} \quad (11)$$

which depends both on the topographic and the mechanical properties of the interface.

The elastic regime is limited to the region  $\psi < 1$ , for which GW have shown that the fraction of plastified contacts is negligible. Persson's more elaborate theory yields a comparable evaluation, with  $s$  and  $R$  in equation (11) now understood to be those on the large scale (upper space cutoff). This last result takes into account consistently the above-mentioned plastification on small lateral scales.

On the other hand, for  $\psi$  larger than a few units, most microcontacts are in a state of full plastic deformation.

<sup>3</sup> The statistical properties of a self affine surface  $z(x, y)$  are invariant under the scaling transformation  $x \rightarrow \zeta x, y \rightarrow \zeta y, z \rightarrow \zeta^{3-D_f} z$ , where  $D_f$  is the fractal dimension.

Multiscale roughness loses relevance, and one may resort to the fully plastic version of the GW model. The matter which has flown being assumed to redistribute on a scale much larger than contact radii (no “piling up”), geometry imposes that the area of a contact involving an asperity with initial compression ( $z - d$ ) is  $2\pi R(z - d)$ . It bears the load  $\pi a^2 H$ , with  $H$  the hardness. Then, trivially

$$\Sigma_r = \frac{W}{H} \quad \bar{a} = \sqrt{2Rs} \quad (12)$$

One may therefore assert the robustness of three characteristics of multicontact interfaces, namely, to a good approximation :

– *The real area of contact is proportional to the normal load, and independent of the apparent area  $\Sigma_{app}$ .*

– *The average contact radius is load-independent, thus introducing a mesoscopic length scale  $\bar{a}$  defined by the topography of the contacting surfaces.*

– *In a wide variety of cases,  $\bar{a}$  is of micrometric order.*

All these statements have been directly confirmed from the analysis, by Dieterich and Kilgore [12], of their optical images of several MCI between transparent solids.

For metals,  $E/Y \sim 10^2$ – $10^3$ . It would therefore take unrealistically small values of  $s/R$ , of order  $10^{-4}$ – $10^{-6}$ , for metal/metal MCI to be in the pure elastic regime. They are fully plastic, as anticipated by Bowden and Tabor.

The opposite case is that of elastomers, which are fully (visco)elastic up to strains  $\gtrsim 1$ . Their interfaces, such as that between tire and road, when analyzed in the frame of Persson’s predictions [20] [21] should provide a test of his theory.

MCI involving polymeric glasses ( $E/Y \sim 10$ – $100$ ) pertain to the intermediate regime, where  $\psi \gtrsim 1$  : a fraction only of the microcontacts flow significantly. Although no quantitative theory is available, we believe that, in view of their robustness, the above-mentioned three main results of the GW model hold for all non-purely elastic MCI. Confirmation of this statement has been provided by experimental investigations of various interfacial properties, such as shear stiffness, which all exhibit the Amontons linear dependence on normal load (see Appendix A).

In fine, we can summarize the above results into the following simple statement for the friction coefficient of a MCI :

$$\mu = \frac{\sigma_s}{\bar{p}} \quad (13)$$

$\bar{p}$  is the average normal stress borne by the microcontacts. It is load-independent. Its expression in terms of the material properties (Young modulus and yield stress) and of the topographic surface characteristics depends upon the value of the plasticity index  $\psi$  (eq.(11)). For

$\psi \gg 1$  (fully plastic regime)  $\bar{p} = H \sim 3Y$ . In the opposite, fully elastic case  $\psi \ll 1$ ,  $\bar{p} \sim E\sqrt{s/R} \sim H/\psi$ , and in the intermediate elasto-plastic range it is expected to extrapolate smoothly with  $\psi$  between these two limits.

Let us insist that the interfacial shear strength  $\sigma_s$  in expression (13), which is likely to depend upon the contact pressure, is load-independent for a given MCI, since such is  $\bar{p}$  itself. This result is specific of multicontact interfaces, for which Amontons’s law is of purely geometric origin. It must be contrasted with the case of intimate single contacts such as those studied with the surface force apparatus (SFA) or extended gel glass ones (see Section III). For these systems, Amontons’s law, when observed, must be attributed to the pressure dependence of  $\sigma_s$  itself [22].

## B. Geometric age : a major state variable for MCI

### 1. Time dependence of the static threshold:

The classical description of solid friction states that there exists, for any given interface, a well defined static friction coefficient  $\mu_s = F_s/W$  such that, as long as the applied shear force  $F < F_s$ , no sliding occurs.

This amounts to asserting that, at a depinning threshold  $F_s$ , the interface commutes from a purely elastic, reversible response to external shearing, to an irreversible, dissipatively flowing one. Most likely, and in view of unavoidable disorder and temperature effects, such a strong statement, which implies that the interface would undergo an abrupt unjamming transition, is only approximate. We come back to this point in § II.C.4, where we discuss in detail the intrinsic difficulties and limits associated with the definition of such a threshold. Let us only state at this point that, in order to minimize ambiguities and make comparison between data meaningful, it is important to define carefully the protocol used to measure  $\mu_s$ .

A series of such *stop and go* experiments consists in :

(i) Preparing the initial interfacial state reproducibly, by sliding steadily at a chosen velocity  $V_{prep}$ , then stopping the pulling.

(ii) Waiting at rest for a given waiting time  $t_w$  under a specified shear stress. This may either be self-selected by the system (natural arrest stress) or imposed at some value below this level.

(iii) Resuming loading at a prescribed velocity  $V_{load}$ , for example  $V_{load} = V_{prep}$ .

A typical shear force response is displayed on Figure 8.  $\mu_s$  is then *conventionally* identified with the peak level. Experiments of this type have been performed on a number of MCI. They reveal that  $\mu_s$  is *not a mere number* characterizing a couple of solids, but a slowly increasing function of the waiting time. More specifically,  $\mu_s(t_w)$  varies logarithmically over several decades of  $t_w$  ranging up from about 1 sec (the typical fast limit for such mechanical experiments). This behavior, displayed on

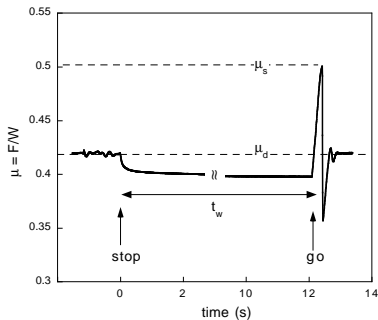


FIG. 8: Friction trace (reduced friction force  $\mu = F/W$  vs time  $t$ ) in a stop and go experiment (see text).  $V_{prep} = V_{load}$ . Interface : PMMA/PMMA at  $T = 300K$ .

Figure 9, holds for a wide variety of materials including metals [23], rocks [5] [24], glassy polymers [25] and paper [9].

*As a MCI ages at rest, it strengthens logarithmically.* Moreover, the slope

$$B = \frac{d\mu_s}{d(\ln t_w)} \quad (14)$$

is found, for all the above-mentioned materials, to be roughly (see Figure 9) on the order of  $10^{-2}$ .

Such a “generic” behavior is striking, and suggests that it results from a robust physical mechanism.

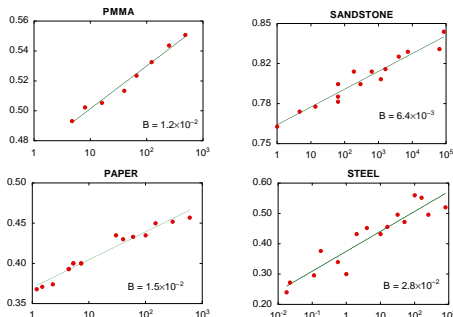


FIG. 9: Static friction coefficient  $\mu_s$  vs waiting time  $t_w$  for symmetric MCIs. Data from : Heslot et al [9] (paper), Baumberger [26] (PMMA), Dieterich [27] (sandstone), Dokos [23] (steel).

## 2. Creep growth of the real area of contact

Tabor’s decomposition of the friction force (eq.(2)), together with the Greenwood-Williamson analysis, immediately raises the possibility that this strengthening might be attributable to slow growth of the real area of contact. Indeed, we have seen that, in general, the average normal stress  $\bar{p}$  borne by the microcontacts is

comparable with the bulk yield stresses of the contacting materials <sup>4</sup>. At this stress level, which prevails in a volume  $\sim a^3$  (with  $a$  the microcontact radius), one expects materials to undergo plastic creep, resulting in the slow growth of microcontacts, hence of  $\Sigma_r$ .

Confirmation of this idea was obtained by Dieterich and Kilgore [12] who were able to measure directly the time evolution of  $\Sigma_r$  on their optical images of the microcontacts forming the MCI between two transparent glassy polymer blocks. They found that  $\Sigma_r(t_w)$  does grow logarithmically, at a rate compatible with that measured in microindentation experiments.

The question is then to ascertain whether or not this area growth is sufficient to explain that of  $\mu_s$ . This has been investigated in detail by Berthoud et al [25]. They studied the temperature dependence of the static aging slope  $B$  for symmetric MCI involving the polymeric glasses PMMA and PS (polystyrene) between room temperature and the vicinity of the bulk glass transitions. They analyzed their results in terms of a model for the growth of  $\Sigma_r$  due to Bréchet and Estrin [28].

This model schematizes the creep-induced growth of a microcontact as follows. Once a microcontact has been created, at time  $t = 0$ , in a first stage of fast plastic flow, of duration negligible on the scale of the later evolution, the normal stress  $\sigma$  sets to an “initial” value  $\sigma_Y$  of the order of the yield stress in the relevant geometry <sup>5</sup>. Once this state is reached, plastic evolution continues via creep, the rate of which is given by an expression à la Nabarro-Herring :

$$\dot{\epsilon} = \dot{\epsilon}_0 \exp \sigma/S \quad (15)$$

where  $\dot{\epsilon}$  is the compressive strain rate (treated as a scalar),  $S$  the so-called strain-rate sensitivity of the flow stress, and  $\dot{\epsilon}_0$  a  $\sigma$ -independent Arrhenius factor. Since this creep law reflects a thermally activated process, both  $\dot{\epsilon}_0$  and  $S$  are  $T$ -dependent.

Such plastic deformation occurs at constant volume, so that :

$$\dot{\epsilon} = \frac{1}{a_0^2} \frac{d(a^2)}{dt} \quad (16)$$

with  $a$  the contact radius,  $a_0$  its initial value. Since  $\sigma = w/\pi a^2 \simeq (1 - \epsilon)w/\pi a_0^2 + \mathcal{O}(\epsilon^2)$ , with  $w$  the normal load. Then, from eqs.(14) and (15), and approximating the MCI by a set of identical average GW contacts, the real area of contact evolves as :

$$\Sigma_r(t) = \Sigma_{r0} \left[ 1 + m \ln \left( 1 + \frac{t}{\tau} \right) + \mathcal{O}(\ln^2) \right] \quad (17)$$

<sup>4</sup> More precisely, for an asymmetric interface,  $\bar{p}$  is on the order of the yield stress of the softer material.

<sup>5</sup> In uniaxial loading,  $\sigma_Y = Y$ , while for a sphere-sphere contact  $\sigma_Y = H \simeq 3Y$  [13].



with

$$m = \frac{S}{\sigma_Y}, \quad \tau = \dot{\epsilon}_0 \frac{1}{m} e^{1/m} \quad (18)$$

Typically, at room temperature, for the systems of interest here,  $m$  values are on the order of a few  $10^{-2}$ . On the other hand, no reliable evaluation of the cross-over time  $\tau$  can be made a priori, due not only to its exponential dependence on  $m$  but even more to the lack of any precise data on  $\dot{\epsilon}_0$ . All MCI studied up to now, except for polymer glass ones close to the glass temperature, exhibit a linear logarithmic growth of  $\mu_s$ , hence of  $\Sigma_r$ , for waiting times above 1 sec. This only enables us to state, at this stage, that in general  $\tau$  is smaller than this limiting value. Then, assuming that the Tabor interfacial shear strength  $\sigma_s$  exhibits no aging, one obtains from eq.(17), in the accessible range  $t \gg \tau$ , for the log-slope of the static friction coefficient :

$$B = \mu_{s0} m \quad (19)$$

where  $\mu_{s0} = \sigma_s \Sigma_{r0}/W = \sigma_s/\sigma_Y$  is the static threshold base value at short times  $t \ll \tau$ <sup>6</sup>. Since friction coefficients of MCI are usually a fraction of unity, one thus expects, at room temperature,  $B$  to lie in the  $10^{-2}$  range.

The analysis of experimental data for  $B(T)$  in ref.[25] is quite intricate, in view of several difficulties concerned with :

- the fact that  $\tau$  and, hence,  $\mu_{s0}$ , could be accessed in the realizable waiting time range only close to the glass transition temperatures  $T_g$ .

- the problems related with mapping the authors' bulk data for  $\sigma_0$  and  $S$  onto the sphere-sphere geometry.

Berthoud et al were nevertheless able to show that expression (19) accounts semiquantitatively for the roughly tenfold increase of  $B$  between its values, of order  $10^{-2}$  at room temperature as expected from expression (19), and the vicinity of the bulk  $T_g$ 's. However, it must be noted that eq.(19) is found to systematically underestimate the experimental data, the relative misfit increasing significantly on approaching  $T_g$ . This hints towards the fact that, while creep-induced growth of the real area of contact is responsible for most of the static strengthening, some aging of the interfacial strength is not completely ruled out : for example, close to  $T_g$ , such symmetric polymer glass contacts might exhibit partial "healing" due to interdiffusion of polymer chains.

Clearly, the Bréchet-Estrin model only describes *plastic* creep of the contacting asperities. However, quasi-logarithmic static aging was also observed by Ronsin et al [30] on rough rubber/rough glass MCIs. For such materials, contact area growth is obviously of viscoelastic origin.

---

<sup>6</sup> Strictly speaking the value of  $\sigma_s$  which appears in this expression should be that at the driving velocity (see §II.C.3 and [29])

We show in Appendix B, following Hui et al [31], that the Greenwood-Williamson model can be worked out explicitly for linear viscoelastic materials, with a very simple outcome. Namely, the GW results (eq.(8)) for the elastic MCI still hold formally, provided that the inverse Young modulus  $1/E$  is replaced by the so-called creep compliance  $J(t)$ , which measures the delayed strain response to a unit instantaneous stress jump. Hence the real area of contact becomes a slowly increasing function of contact duration. A logarithmic increase is known to provide a reasonable approximation for  $J(t)$  over time decades, for materials with a very wide spectrum of relaxation times such as rubbers.

### 3. Geometric age as a dynamical state variable

In the light of the foregoing analysis we will for the moment attribute the strengthening of MCI static thresholds to the sole time dependence of the area factor in Tabor's expression.  $\Sigma_r$  thus becomes a function of the *geometric age of the interface*  $\phi$  by which  $t$  should now be replaced in equation (17). More precisely, this age is defined as follows.

- For a non-moving MCI,  $\phi(t)$  is simply the time which has been spent at rest at time  $t$ .

- Consider now a MCI sliding at the constant velocity  $V$ . As motion proceeds, a given microcontact, once created (born) is gradually sheared until it slides, then disappears (dies) when the relative displacement between the partner asperities reaches a value on the order of a fraction of the contact diameter. Since, under constant normal load, the average number of microcontacts is conserved, any contact death is, on average, associated with the birth of a new microcontact at an uncorrelated position. Since  $\Sigma_r \ll \Sigma_{app}$ , we can safely consider that the newborn is formed between fresh asperities, which have not yet experienced creep<sup>7</sup>.

Contact renewal therefore limits the age of the MCI to the average lifetime of a given configuration of microcontacts, which can be written phenomenologically as :

$$\phi_{ss} = \frac{D_0}{V} \quad (20)$$

In other words, *motion interrupts aging*, since interfacial configuration memory is destroyed after sliding the *characteristic length*  $D_0$ , which we expect to lie in the micrometer range.

Note that the larger  $V$ , the younger the steady sliding MCI, hence the smaller  $\Sigma_r(\phi)$ : geometric aging thus immediately appears as a candidate process for explaining

---

<sup>7</sup> This approximation, which neglects wear, is validated by the observed stability of the frictional characteristics of a MCI over slid lengths as large as a few 10 cm [32] – a distance over which we can estimate the number of contact configuration renewals to  $10^{4-5}$ .

the  $V$ -weakening behavior of the steady sliding dynamical friction coefficient  $\mu_d(V)$  mentioned in Section I.

• Let us now turn to non-steady sliding at the instantaneous velocity  $\dot{x}(t)$ .  $\phi$  is no longer time-independent, since it keeps track of geometric aging over the time necessary to slide the memory length  $D_0$ . In this sense,  $D_0$  is the length over which memory of the history of motion is preserved.

The most simple phenomenological expression for  $\phi$  accounting for this behavior is :

$$\phi(t) = \int_{t_0}^t dt_1 \exp\left[-\frac{(x(t) - x(t_1))}{D_0}\right] \quad (21)$$

where  $t_0$  is the time at which the two solids were first brought into contact. Note that, in agreement, as needed, with the previously defined expressions. :

– for the static MCI equation (21) yields  $\phi(t) = (t - t_0) \equiv t_w$ ,

– steady sliding corresponds to the limit  $t_0 \rightarrow -\infty$ , so that  $\phi(t)$  as defined from eq.(21) reduces to the constant  $\phi_{ss}(V) = D_0/V$ ,

Geometric age thus becomes a dynamical variable, coupled to the instantaneous velocity  $\dot{x}(t)$  by the non-linear differential equation, equivalent to expression (21):

$$\dot{\phi} = 1 - \frac{\dot{x}\phi}{D_0} \quad (22)$$

which was first proposed by Rice and Ruina [6].

That the memory of the interfacial state of sliding MCIs is indeed characterized by a length, a possibility first suggested by Rabinowicz [33] in an often overlooked pioneer work, was established by Dieterich [5] on the basis of his systematic exploration of frictional transients following velocity jumps. In these experiments the slider is set into steady motion by driving it, through a “spring” of stiffness  $K$ <sup>8</sup>, at an initial velocity  $V = V_i$ . At  $t = 0$ ,  $V$  is suddenly jumped to  $V_f$ , and one measures the force response. As can be seen on Figure 4, this exhibits a two-step transient.

(i) In a first, very rapid stage, for upward (resp. downward) velocity jumps, the instantaneous dynamic friction coefficient increases (resp. decreases).

(ii) This so-called “direct effect” is followed by a much slower monotonous variation in the reverse direction, ending at the level  $\mu_d(V_f)$ .

Dieterich found that the duration of the transient, which is dominated by that of stage (ii), scales as  $1/V_f$ . From this he identified a value of  $D_0 \simeq 5\mu\text{m}$  for a granite/granite MCI. One may then conclude that the slow part of the transient corresponds to the gradual relaxation of the real contact area from its

initial steady value  $\Sigma_r(\phi = D_0/V_i)$  towards its final one  $\Sigma_r(\phi = D_0/V_f)$ .

In conclusion of this analysis, it appears reasonable to write tentatively Tabor’s expression as :

$$F = \Sigma_r(\phi) \sigma_s(\dot{x}) \quad (23)$$

which assigns the whole state dependence to the area factor, while assuming that the shear strength  $\sigma_s$  only depends on the instantaneous sliding velocity. The validity of this assumption will be discussed at length in the forthcoming sections.

Equations (23) and (22), together with Newton’s equation :

$$M\ddot{x} = F_{drive}(x, t) - F(\phi, \dot{x}) \quad (24)$$

where  $F_{drive}$  is the externally applied driving force, provide a closed set of equations for the frictional motion of the slider once the form of the functional  $\dot{x}$ -dependence of  $F$  has been identified.

### C. Junction rheology : gross features

#### 1. Junctions at multicontact interfaces

Up to now, we have concentrated on the analysis of the contact geometry of MCI which, though an important prerequisite, does not yet touch upon our main question, namely that of the origin of frictional dissipation and of the detailed nature of the associated rheology described by the interfacial shear strength  $\sigma_s$ . Let us first try to identify the regions which are the seat of frictional dissipation.

We have restricted our definition of MCI to the normal load range such that microcontacts are numerous enough to form a good statistical set, but sparse enough for elastic interactions between them via the bulk materials to be negligible. This entails that we can now simply focus on the behavior of a single sheared microcontact. Such a unit (Figure 10) is constituted of the bulk of the two asperities and of an interfacial layer in which molecules from both surfaces have come into adhesive contact.

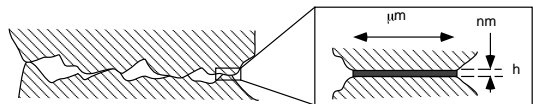


FIG. 10: Each microcontact is formed by a nm-thick adhesive junction between the two asperity bulks.

This layer, which we call the *junction*, has a disordered structure. This is obvious when the two solids are polymer glasses, since in this case the junction is formed

<sup>8</sup> More precisely,  $K$  is the equivalent stiffness of the driving stage plus slider system.

by polymer tails and loops protruding from the amorphous bulks. In the case of crystalline bulks, structural and chemical surface disorder, which prevails under usual (non atomically planar and non ultra high vacuum) conditions together with plastic smoothing out of nano-scale roughness certainly lead to structural disorder.

Such highly defective structures, probably less dense than the bulks, are likely to result in lower resistance against plastic shear deformation. So, we will assume that *the junction is a disordered quasi bidimensional medium with thickness  $h$  in the nanometric range, where shear naturally localizes*. We will show that this assumption is borne out by the analysis of experimental data on low velocity friction.

## 2. A threshold rheology

Stating the existence of a well-defined static friction coefficient can be formulated equivalently as the fact that, when the sliding velocity  $V \rightarrow 0$ ,  $\sigma_s$  does not vanish, but tends towards a finite limit  $\sigma^*$ . That is, from a rheological viewpoint, frictional contacts behave as yield stress fluids.

*The yield stress  $\sigma^*$  therefore appears as the threshold beyond which the interfacial quasi-2D solid flows plastically.*

At lower stress levels, in this simple picture, the interface does not slide, it is pinned and responds to shear as a solid i.e., in principle, elastically. Due to the nanometric thickness of the junctions, the corresponding stiffness is always much larger than that of the microcontact-forming asperities themselves (see Appendix A)<sup>9</sup>, it is therefore not accessible in MCI configurations.

It is common knowledge that plastic flow does not set in as an ideally sharp transition : at non-zero temperatures, thermal activation induces creep below the nominal yield stress, which can be attained, in principle, only by loading at extremely high rates. In other words, the smaller the loading rate, the more fuzzy the threshold. So, one expects that a constant shear load close below the static threshold should induce creep-like frictional sliding. This was indeed observed by Heslot et al [9].<sup>10</sup>

## 3. Beyond threshold : rate effects

*a. Velocity jumps : the direct effect.* We already mentioned in §II.B.3 that the force response (see Figure 4) to a jump of the driving velocity from  $V_i$  to  $V_f$

exhibits, previous to the slow transient attributable to geometric age adaptation, a first much faster part. The associated force jump  $W\Delta\mu_d$  is positive (resp. negative) for  $V_f > V_i$  (resp.  $V_f < V_i$ ), hence the term “direct effect”. Dieterich has shown that :

$$\Delta\mu_d(V_i \rightarrow V_f) = A \ln \left( \frac{V_f}{V_i} \right) \quad (25)$$

where  $A$  is a constant for a given couple of materials. Its values lie in the  $10^{-2}$  range. This holds for all the MCI studied up to now, for velocities between about 0.1 and  $100\mu\text{m}\cdot\text{sec}^{-1}$ .

Note that, as long as inertia is negligible, motion is quasi-static, i.e. after the jump at  $t = 0$  :

$$K(V_f t - x) = W [\mu_d(\phi, \dot{x}) - \mu_d^{st}(V_i)] \quad (26)$$

$x(t)$  measures the position of some reference point on the slider along the pulling direction,  $x(0) = 0$ , and  $\mu_d^{st}(V) = \mu_d(D_0/V, V)$  is the friction coefficient for steady sliding at velocity  $V$ .

The peak value of the transient force ( $d\mu_d/dt = 0$ ) therefore occurs for  $\dot{x} = V_f$ . Velocity jump experiments are performed with as stiff as possible driving stages such that, as can be checked by direct measurements, the distance slept during the fast part of the transient be much smaller than the memory length  $D_0$ . Under such conditions the corresponding variation of geometric age from its initial value  $\phi_i = D_0/V_i$  is negligible, and the direct effect is fully attributable to the rate dependence of the shear strength  $\sigma_s$ .

From equation (23) one then expects that :

$$\Delta\mu(V_i \rightarrow V_f) = \frac{\Sigma_r(D_0/V_i)}{W} [\sigma_s(V_f) - \sigma_s(V_i)] \quad (27)$$

That is, making use of equations (17) and (25)

$$\Delta\sigma_s = \sigma_s(V_f) - \sigma_s(V_i) = \frac{A \ln(V_f/V_i)}{\Sigma_{r0} \left[ 1 + m \ln \left( 1 + \frac{D_0}{V_i \tau} \right) \right]} \quad (28)$$

Since  $m \sim 10^{-2}$ , the log term in the denominator can be neglected, and  $\Delta\sigma_s \simeq \frac{AW}{\Sigma_{r0}} \ln \left( \frac{V_f}{V_i} \right) = A\sigma_Y \ln \left( \frac{V_f}{V_i} \right)$ , from which we can write the following empirical expression for  $\sigma_s$  :

$$\sigma_s(\dot{x}) = \sigma_{s0} \left[ 1 + \alpha \ln \frac{\dot{x}}{V} + \mathcal{O}(\ln^2) \right] \quad (29)$$

with

$$\alpha = \frac{A\sigma_Y}{\sigma_{s0}} \quad (30)$$

<sup>9</sup> A rough estimate for the corresponding ratio is  $\bar{a}/h \gtrsim 10^3$ , with  $\bar{a}$  the average microcontact radius,  $h$  the junction thickness.

<sup>10</sup> Note, however, that with MCI this creep is certainly amplified by the geometric rejuvenation (weakening) associated with sliding.

and  $\sigma_{s0} \equiv \sigma_s(V_0)$  is the shear strength at the reference velocity  $V_0$ , which may be chosen anywhere in the range  $(0.1 - 100 \mu\text{m}/\text{sec})$  where equation (25) holds.

The necessity of resorting to an expression involving a finite reference velocity is imposed by the formal divergence of the logarithm in the vanishing  $\dot{x}$  limit. This divergence is of course unphysical and only points out the limits of the empirical approach. We will return to this point later, when discussing the behavior to be expected for  $\sigma_s(\dot{x})$  in the very low and large velocity regimes.

Note finally that  $\sigma_{s0}/\sigma_Y$  is the friction coefficient  $\mu_{s0}$  appearing in equation (19), it is therefore roughly of order 1 and, in order of magnitude :

$$\alpha \sim A \sim 10^{-2} \quad (31)$$

*b. Steady sliding friction coefficient.* The velocity jump experiments initiated by Dieterich have played a pioneering role to evidence the state and rate character of MCI friction and to separate clearly the age (state) and rheologic (rate) contributions to the dynamic friction coefficient  $\mu_d$ . However, it is the studies of the velocity and temperature dependences of  $\mu_d(V)$  under steady sliding conditions which have led to a systematic confirmation of the validity of expression (29) and opened the way to its more quantitative explication.

The typical experimental  $V$ -dependence of  $\mu_d$  is illustrated on Figure 11, on the cases of granite, paper and PMMA symmetric MCI at room temperature. It is seen that :

(i)  $\mu_d$  is  $V$ -weakening ( $d\mu_d/dV < 0$ ) in the whole low velocity regime explored in such experiments.

(ii) Its variations are quasi-logarithmic, except in the higher  $V$  range ( $V \sim 100 \mu\text{m}/\text{sec}$ ) where it exhibits a saturating trend. For all materials, the log-slope  $\beta_d = -d\mu_d/d(\ln V)$  lies, once more, in the  $10^{-2}$  range.

Such results can be confronted with the predictions obtained from equations (23), (17) and (29) which yield, in steady motion where the geometric age  $\phi = D_0/V$  :

$$\begin{aligned} \mu_d(V) &= \frac{\sigma_{s0}}{\sigma_Y} \left[ 1 + m \ln \left( 1 + \frac{D_0}{V\tau} \right) + \alpha \ln \frac{V}{V_0} \right] \\ &= \frac{\sigma_{s0}}{\sigma_Y} + B \ln \left( 1 + \frac{D_0}{V\tau} \right) + A \ln \frac{V}{V_0} \end{aligned} \quad (32)$$

where we have taken advantage of the smallness of  $m$  and  $\alpha$  to neglect the  $\mathcal{O}(\ln^2)$  terms, and made use of equations (19) and (30).

For  $V \ll D_0/\tau$ , equation (32) gives for the log-slope of  $\mu_d$  the value :

$$\beta_d = B - A \quad (33)$$

The fact that  $\beta_d$  is positive entails that, *at room temperature*,  $B > A$ . Moreover, the  $\beta_d$  data are found to be quantitatively compatible with the available independently measured  $B$  and  $A$ .

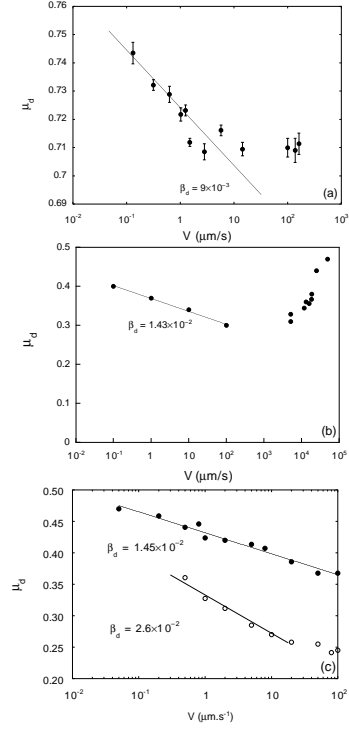


FIG. 11: Dynamic friction coefficient  $\mu_d$  versus steady sliding velocity  $V$  for symmetric MCI : (a) granite (data from [34]) (b) paper (data from [9]) (c) PMMA at  $T = 296^\circ\text{K}$  (full symbols) and  $T = 384^\circ\text{K} \simeq T_g$  (empty symbols) (data from [29]). Due to the increase of the crossover time  $\tau$  (see eq.(18)) with  $T$ , close below  $T_g$ ,  $V_{min}$  has decreased enough to lie in the experimental range.

On the other hand, the saturating trend at the larger  $V$ 's appears as resulting from that of the real area of contact in the small age limit, which becomes relevant for  $V \gtrsim D_0/\tau$ . More precisely, equation (32) predicts a broad minimum of  $\mu_d$ , which should occur for  $V_{min} = (D_0/\tau)(B - A)/A \approx D_0/\tau$ .

That is, expression (32) predicts that, beyond  $V_{min}$ , dynamic friction should become *velocity-strengthening*. This natural physical consequence of the nature of geometric aging, which has been checked experimentally on the case of paper [9], has been overlooked up to now in most studies of fault dynamics. It is important in view of its bearing upon the nature of the sliding dynamics.

We have seen in §II.B.2 that parameter  $B$  varies with temperature in a way which is explained by its physical origin – the thermally activated creep of  $\Sigma_r$ . On the same polymer glass systems, Berthoud et al have shown [29] that  $A$  increases quasi-linearly<sup>11</sup> when increasing  $T$  up to the vicinity of  $T_g$ . Blanpied et al [35] and Nakatani [36] have investigated the behavior of, respectively,  $\beta_d$

<sup>11</sup> Note, however, that the  $T$ -range in these experiments is small.

and  $A$  for granite over wide  $T$ -ranges, from room temperature to  $800^\circ\text{C}$  (still well below the melting point).  $\beta_d$  was found to decrease with increasing  $T$ , enough for hot granite to become velocity-strengthening – a point of importance in the context of deep seismicity.  $A$ , on the contrary, increases in a quasi-linear manner. We defer a more detailed analysis and interpretation of these results, in particular those concerned with  $A$ , to § II.C.4 below, where we propose a physical model for the rate effect.

#### 4. Threshold rheology as a signature of multistability

The primary feature of frictional rheology is the existence of a threshold. That is, the force  $F$  needed for an interface to slide at velocity  $V$  remains finite for vanishing  $V$ 's. This is obviously at odds with the standard picture of dissipation at low rates, namely : if the externally imposed rate of shear is much smaller than the internal relaxation ones, the system evolves *quasi-adiabatically*, so that dissipation vanishes linearly with  $v$ . As first formulated by M. Brillouin in 1904 [37], in order for  $F$  to exhibit a finite threshold, it is therefore necessary that, however slow the drive, the sheared medium evolves through a succession of adiabatic adaptation periods intersped with fast instability events. Each of these events then corresponds, even at vanishing  $v$ , to a finite energy loss, thus accounting for the threshold behavior.

In modern language, *a threshold rheology implies multistability*, as has been developed at length in various fields such as magnetic hysteresis, wetting dynamics, charge density wave and type-II superconducting transport [38].

##### a. A toy model for junction rheology

Let us first illustrate this idea here on a toy model of a sheared junction<sup>12</sup>. We represent it, as shown on Figure 12, as formed by a set of identical blobs of elastic matter attached to two stiff plates with vertical separation  $h$ , and area  $\Sigma$ . The blobs are randomly distributed along the surfaces of these plates, and form  $n$  contacts per unit area. They compress each other when making contact, in which case they interact via the (repulsive) pinning potential  $U(x)$ , where  $x$  measures their relative position along the shearing direction (Figure 12). As  $x$  is increased, some contacts are being destroyed while others are created at random positions, so that  $n$  remains

constant. We assume, for simplicity, that horizontal displacements are purely one-dimensional.

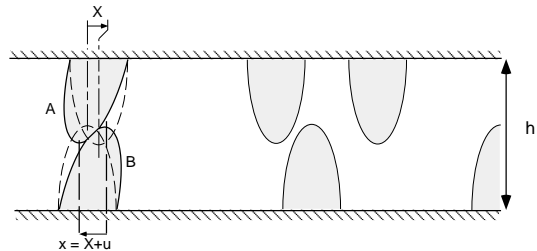


FIG. 12: (a) Toy model of the adhesive junction.  $X$  denotes the relative displacement of blob **A** with respect to **B** in the absence of shear compliance ( $k = 0$ ),  $x = X + u$  the real relative coordinate of the shear-deformed **A/B** contact. (b) The repulsive interblob potential  $U(x)$ .

The system is sheared by imposing to the upper plate the displacement  $X$  with respect to the lower one. Let  $k$  be the shear stiffness of the system formed by two contacting blobs. Under the action of the pinning potential, the center of each blob contacting surface undergoes an elastic shear displacement  $u/2$  along  $Ox$ , so that the horizontal separation  $x = X + u$ . The total energy of a contact is thus :

$$\mathcal{E}(X, u) = U(X + u) + \frac{1}{2} ku^2 \quad (34)$$

Assume for the moment that  $T = 0$ . Then, for fixed  $X$ ,  $u$  sets at the value  $u^*(X)$  which minimizes  $\mathcal{E}$ , such that :

$$U'(X + u^*) = -ku^* \quad (35)$$

Two cases must then be distinguished, depending on whether the instantaneous equilibrium thus defined is unique (monostable contact) or not (bistable contact).

##### Monostable contact:

If  $k > k_0 = \max(-U'') \sim U_0/a^2$ , – with  $a$  the range of  $U$ ,  $U_0$  its maximum value – the solution of eq.(35) is unique whatever the value of the reference coordinate  $X$  (see Figure 13).

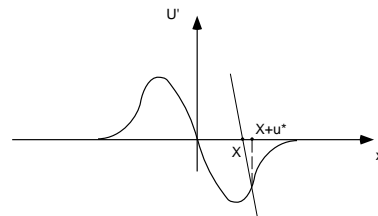


FIG. 13: Graphical solution of the local equilibrium equation (35) in the monostable case.

<sup>12</sup> This model was first developed by Caroli and Nozières [39]. Although their formal results directly apply here, let us point out that the original physical interpretation – that the elementary mechanically unstable units were the interasperity microcontacts as a whole – was not correct [40]. Let us insist again that *the relevant instabilities do not occur on the micrometric scale but, within the inter-asperity junction, on the nanometric scale.*

Assume that we impose a constant external shear velocity  $\dot{X} = V$ . As  $X$  increases,  $u$  nearly follows its instantaneous equilibrium value  $u^*(X)$ , and the contact energy evolves as  $\mathcal{E}^*(X) \equiv \mathcal{E}(X, u^*(X))$ . Indeed, the excess elastic energy is dissipated out of the contact region of size  $\sim a$  via acoustic radiation, at the characteristic rate  $\tau_{eq}^{-1} \sim c/a$ , with  $c$  a sound velocity, hence much larger than the shear rate  $\dot{\gamma} \sim V/h \sim V/a$ .

The instantaneous pinning force exerted by the contact on the upper plate is simply :

$$f_p = -\frac{d\mathcal{E}^*}{dX} = -\left.\frac{\partial\mathcal{E}}{\partial X}\right|_{u=u^*} - \left.\frac{\partial\mathcal{E}}{\partial u}\right|_{u=u^*} \frac{du^*}{dX} \quad (36)$$

i.e., taking advantage of eq.(35)

$$f_p(X) = -U'(X + u^*(X)) \quad (37)$$

and the net work spent to sweep through the contact :

$$w = -\int_{-\infty}^{\infty} dX f_p(X) = U(X + u^*)\Big|_{-\infty}^{\infty} = 0 \quad (38)$$

The total instantaneous friction force  $F(V)$  for a junction of area  $\Sigma$  is the sum of the pinning forces  $f_p$  over the  $n\Sigma$  randomly positioned contacts of transverse range  $a$ , so that :

$$F = \frac{n\Sigma}{a} \int_{-\infty}^{\infty} dX (-f_p(X)) = n\Sigma \frac{w}{a} = 0 \quad (39)$$

As could be expected, for an elastically monostable junction, frictional dissipation vanishes when  $V \rightarrow 0$ .

### Bistable contact :

In the opposite case where  $k < k_0$ , in a finite range of values of  $X$  equation (35) has three solutions  $u_i^*(X)$  (Figure 14), the two extreme ones  $u_{1,2}^*$  corresponding to minima  $\mathcal{E}_{1,2}^*(X)$  of the energy  $\mathcal{E}(X, u)$ , while  $u_0^*$  is associated with a maximum. As  $X$  is slowly increased from  $-\infty$ , the instantaneous  $u^*$  evolves continuously with  $\mathcal{E}$ , i.e. follows branch  $u_1^*$  (Figure 14b). The  $\mathcal{E}_1^*$  equilibrium gradually evolves from fully to meta-stable, while the barrier  $\Delta\mathcal{E}_b(X)$  separating the two basins of  $\mathcal{E}$  decreases until the spinodal limit  $X = X_+$  where it vanishes. At this bifurcation point, branch (1) terminates,  $u_1^*$  becomes unstable, and the only choice for the system is to relax towards the, now single, lower minimum  $\mathcal{E}_2^*$ . The corresponding finite energy difference  $\Delta\mathcal{E}_{12}$  is, again, lost via acoustic radiation, i.e. instantaneously on the scale of the drive. The pinning force  $f_p$  exhibits the hysteresis cycle common to such bistable systems (Figure 14c). The work for sweeping through the contact (the hatched area noted (1) on Figure 14c)  $w = \Delta\mathcal{E}_{12}$  is now finite.

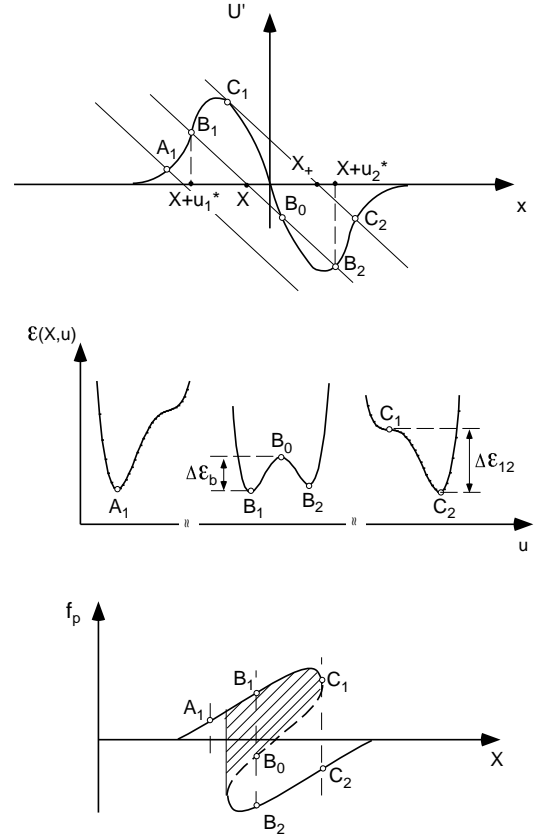
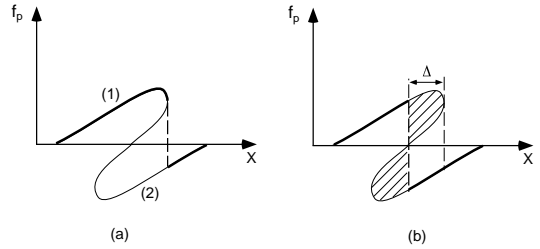


FIG. 14: (a) Local equilibrium construction for a bistable contact for various values of the reference coordinate  $X$ . (b) Evolution of the contact energy  $\mathcal{E}(X, u)$  for increasing  $X$ . The extrema correspond to the intersections labelled in (a). (c) Pinning force cycle for the bistable contact. When driven towards increasing  $X$ , the system follows branch (1) up to  $C_1$ , where it jumps down to  $C_2$ .

The friction force  $F$  on the whole junction corresponds to a random distribution of  $X$ , i.e. to a uniform population  $P(X)dX = n\Sigma dX/a$  of branch (1) of the hysteresis cycle (Figure 15a), so that  $F_a = n\Sigma w/a$ . Multistability results in a threshold rheology and, as long as  $V \ll c$ , the dynamic friction force is velocity independent<sup>13</sup>.



<sup>13</sup> The corrections resulting from imperfect adiabatic adaptation are easily shown to be of relative order  $(V/c)^{2/3}$  [39]

FIG. 15: The thick lines correspond to the populated parts of the force cycle for (a) the sliding junction (b) the junction at rest after turning off the shearing force.  $\Delta$  is the associated rigid recoil.

Let us now assume that, starting from this steady sliding regime, we suddenly suppress the external shear force. The interblob contacts must react so as to bring the system to global mechanical equilibrium, where the sum of the pinning forces vanishes. The only way for the junction to realize this situation is via a recoil  $\Delta$  of the upper plate : each individual reference coordinate  $X_i$  decreases to  $(X_i - \Delta)$ , yielding a new distribution  $P_{eq}(X)$  such that the two shaded areas on Figure 15b be equal.  $P_{eq}$  has a discontinuity at the Maxwell plateau of the force cycle. If, starting from this state, we now gradually increase the external shear force  $F$ ,  $P_{eq}$  rigidly shifts to the right by  $\delta X(F)$ . As long as  $\delta X < \Delta$ , no irreversible “jump” occurs, the displacement is therefore fully reversible : the junction is in an elastic regime. This terminates when the discontinuity of the shifted distribution reaches the spinodal limit  $X_+$ , i.e. when  $\delta X = \Delta$ , i.e.  $F = F_d$ . In this stop and go scenario, the static threshold force is equal to the dynamic one.

However, due to multistability, global equilibrium can be realized by a huge number of configurations of the interblob contacts. Let us assume that we create the un-sheared junction by bringing the two plates into contact. Depending on the details of this “mechanical quench”, each newly formed interblob contact may correspond to a state on either of the two branches of the force cycle, the only condition to be satisfied being that :

$$\int dX \sum_{i=1,2} P_i(X) f_{pi}(X) = 0 \quad (40)$$

where  $i$  labels the branches of the force cycle. The elastic regime ends when the edge of the shifted  $P_1$  reaches  $X_+$ . This point, where irreversible sliding starts, is the static threshold. Contrary to dynamic friction, *it is not an intrinsic property of the junction but depends on its past history*. If, for example,  $P_1(X_+) \neq 0$ , dissipation starts at vanishingly small shear. This has been illustrated in ref. [41] where it was shown that the dispersion in measured values of  $\mu_s$  for a PMMA MCI is strongly reduced by preparing the initial state in a controlled way, i.e. by sliding before repose.

### Rate effect at finite temperature :

Consider a bistable contact, swept along branch 1 of the force cycle, i.e. sitting at the left minimum of the  $\mathcal{E}(u)$  potential (Figure 14). As soon as  $T \neq 0$ , thermal noise is able to activate jumps over the barrier  $\Delta\mathcal{E}_b(X)$ , i.e. to provoke *premature jumps* onto branch 2 before the spinodal limit  $X_+$  is reached. For fixed  $X$ , the jumping rate is the Kramers one :

$$\frac{1}{\tau(X)} \approx \omega_a \exp \left[ -\frac{\Delta\mathcal{E}_b(X)}{k_B T} \right] \quad (41)$$

with  $\omega_a$  an attempt frequency, here typically  $\approx c/a$ . As  $X$  approaches  $X_+$ ,  $\Delta\mathcal{E}_b$  decreases smoothly to zero, and  $\tau(X)$  decreases exponentially up to a cut-off fixed by viscous (acoustic) dissipation. In practice, only close below the spinodal limit does the activated jumping rate become non negligible. The steady sliding distribution  $P$  is now controlled by the competition between :

- the advection imposed by the external drive of  $X$  at velocity  $V$ ,
- the thermally induced jumps from branch 1 to branch 2.

This is expressed by the evolution equation <sup>14</sup>:

$$\frac{\partial P}{\partial t} = -V \frac{\partial P}{\partial X} - \frac{P}{\tau(X)} \quad (42)$$

the steady solution  $P_{st}$  of which reads :

$$P_{st}(X) = Const \exp \left[ -\int_{-\infty}^X \frac{dX'}{V\tau(X')} \right] \quad (43)$$

Due to the exponential variation of  $\tau$ ,  $P_{st}$  is quasi-completely depleted between  $X_+$  and a cut-off  $X_c$  below which activation plays a negligible role. The friction force is thus smaller than its  $T = 0$  limit. Moreover, the larger  $V$ , the less time the contact spends in the vicinity of a given  $X$ , the less the probability for it to jump prematurely. Hence,  $X_c$  increases with the driving velocity, and the friction force increases accordingly : *thermal noise results in a velocity-strengthening rheology*.

This rate dependence can be evaluated analytically as long as the barrier height evolution for  $X \sim X_c$  can be approximated simply. For not too large  $V$ , where variations are linear, it is found (see ref. [3], Chapter 11) that :

$$F(V) = F(V_0) \left[ 1 + \alpha_{th} \ln \left( \frac{V}{V_0} \right) \right] \quad (44)$$

with  $V_0$  is a reference velocity in the above-mentioned range of validity, and :

$$\alpha_{th} = \frac{k_B T}{\bar{\sigma} v_{act}} \quad (45)$$

and  $\bar{\sigma} \simeq nw/a$  is on the order of the  $T = 0$  frictional stress. At larger velocities, when  $X_c$  comes very close

<sup>14</sup> This expression assumes implicitly that the drive is slow enough for the instantaneous jumping rate to be that for the non-advised system

below  $X_c$ ,  $\Delta\mathcal{E}_b \sim (X_c - X)^{3/2}$ , and the rate dependence of  $F$  commutes from log-linear to  $(\ln V)^{2/3}$  [39] - a behavior which has been observed by Sills and Overney [42] in a nanoscale friction experiment on glassy polystyrene performed with an atomic force microscope.

*b. From the toy model to the real junction :*

When noticing that the functional form predicted by the toy model (eq.(44)) for the interfacial rheology does fit the empirical expression (eq.(29)) deduced from experiments, one is led to go one step further. That is, let us take for a moment the toy model at face value and compare experimental results for coefficient  $\alpha$  (eq.(30)) with  $\alpha_{th}$  (eq.(45)). As mentioned above, Nakatani [36] found that, for granite,  $\alpha$  increases quasi-linearly with temperature, in agreement with equation (45) - a result confirmed for PMMA in the more restricted velocity range investigated in [29]. These authors have then been able to deduce values of the volume  $v_{act}$ . In both cases, they find it to be on the order of a few  $\text{nm}^3$ .

This naturally leads to conclude that, inspite of its crudeness, the toy model does capture the main physical mechanisms responsible for the frictional rheology of MCI, namely :

(i) When sheared, the highly confined junctions between asperities are the seat of mechanical instabilities, each of which primarily affects a small region containing a few atomic (or, for polymer glasses, monomer) units.

(ii) The strengthening, logarithmic, rate effect can be assigned to premature “flips” of these clusters induced by *thermal* noise.

Feature (i)) is fully consistent with our description of the junction as a quasi-2D disordered medium, solidified under the high confinement conditions imposed by the bulks of the contacting asperities, but mechanically weaker than these bulks - probably due to a higher fraction of quenched free volume. Indeed, a number of numerical studies, pioneered by Argon et al [43] (see also Falk and Langer [44] and Malandro and Lacks [45]) of sheared glasses, both polymeric and molecular, at temperatures  $\ll T_g$ , have shown that elastic dissipation in these systems occurs essentially via sudden collective rearrangements of clusters of typically nanometric volume. These clusters, termed by Falk and Langer shear transformation zones (STZ), are randomly located<sup>15</sup> and their average density is constant at constant shear rate  $\dot{\gamma}$ <sup>16</sup> : on average, once a STZ has flipped into a lower energy local equilibrium state, another one appears at an uncorrelated position. That is, we may interpret the interblob bistable contacts of the toy model as a sketchy representation of STZ's, the volume  $v_{act}$  providing a rough evaluation of the average zone volume.

Feature (ii) opens onto a much more difficult, still essentially unsolved question. In the toy model, the bistable units are completely decoupled, and their contributions to the friction stress are simply additive. The real junction is, of course, dense everywhere, so that each STZ must be understood as embedded in a quasi-2D elastic medium, and coupled to the adjacent deformable asperity bulks which, though stiffer, do transmit stresses. The flip of a STZ is therefore akin to the transformation of an Eshelby inclusion [46]: as already emphasized in [43], it gives rise to a multipolar force signal which deforms the surrounding medium [47], hence resulting in loading steps on the other STZ's, which were “on their way towards flipping”. The randomness of these signals in time and space is the source of the so-called *dynamic noise*, which acts in parallel with the thermal one. Elastic coupling being long ranged, dynamic noise is likely to trigger cascades (avalanches) of correlated flips, which are not accounted for in mean field approximations - hence the difficulty of this class of problems [38].

Moreover, clearly, the larger the imposed strain rate  $\dot{\gamma}$ , the more frequent the flips hence, roughly speaking, the larger the effective strength of the dynamic noise - which must vanish in the vanishing  $\dot{\gamma}$  limit. So, if these effects can be modelled in terms of an effective temperature, this must be a growing function of  $\dot{\gamma}$ . Up to now, no theory of this effect is available, and it is therefore not taken into account by the recent phenomenological theories of plasticity of amorphous media : the STZ-based one [44] and the soft glass rheology of Sollich et al. [48]. Qualitatively, one expects such rheologies to exhibit a crossover between two limiting regimes : a thermal noise-controlled one at low  $\dot{\gamma}$  and/or high  $T$ , a dynamic noise-controlled one in the opposite conditions.

Our above analysis of friction leads us to conclude that *the rheology of MCI junctions is controlled, at and above room temperature, by thermal noise, in the investigated range of  $\dot{\gamma} = V/h$  i.e. typically  $\dot{\gamma} \lesssim 10^5$ .*

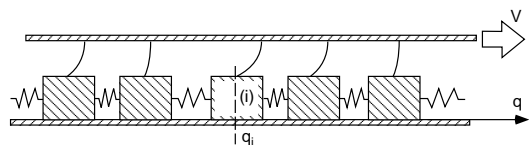


FIG. 16: Schematic representation of Persson’s model [3]. The junction is constituted of a dense set of elastically coupled nanoblocks driven by a rigid plane through shear springs. When the stress on a block  $\sigma < \sigma_a$ , it is stuck to the lower plate. When  $\sigma$  reaches  $\sigma_a$  it gets depinned and performs damped motion. When its sliding velocity  $\dot{q}_i$  vanishes it re-sticks.

Persson has studied numerically a model which represents the junction, as sketched on Figure (16), as a dense set of elastically coupled pinned blocks driven by a rigid plate. He found (see [3], chap. 11) that dynamic noise effects were negligibly small, thus justifying a thermal noise-controlled mean field rheology (equation

<sup>15</sup> In the absence of shear localization

<sup>16</sup> To which extent and how this density depends on  $\dot{\gamma}$  is an important though still unsettled question.



(44)). Note however that the smallness of dynamic noise effects in his model is likely to result from the infinite stiffness of the confining plates, which should lead to exponential screening of elastic couplings.

Our analysis of MCI rheology can therefore be summed up by the artist's view of Figure (17). The "threshold-plus-logarithmic" behavior fitted by the toy model results should therefore be understood as corresponding to an intermediate regime, with limits on both the high and low velocity sides.

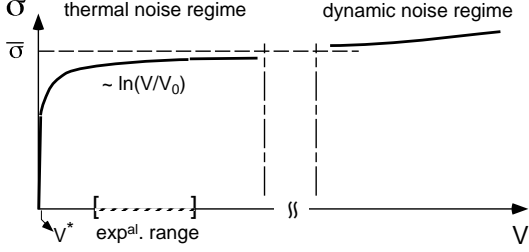


FIG. 17: Schematic interfacial stress *vs* velocity curve (see text). The Newtonian Eyring regime corresponds to  $0 < V < V^*$ .

In view of the current high activity in the field of soft glass rheology, one may be optimistic about the emergence of theoretical predictions about the position of the high- $V$  crossover towards the non thermal regime. However, it must be pointed out that MCI friction is certainly not a good tool for experimental investigation of this question since, at the necessary sliding velocities, in the mm/sec range or larger, one would have to cope with the tricky problems related with e.g. frictional heating.

The opposite low- $V$  limit is essentially academic. Let us come back to the toy model : as the stress decreases, the cut-off  $X_c$  of the contact distribution approaches form above the position corresponding to the Maxwell plateau, and the rate of back jumps from branch 2 to 1 becomes non negligible and comparable with the  $1 \rightarrow 2$  one. At the same time, the interbranch barrier  $\Delta\mathcal{E}_b$  increases to  $\sim \sigma_Y v_{act}$ , making jumps extremely rare. This results in the classical Eyring (*sinh*) behavior for  $\sigma_s(V)$ , ending in an extremely fast quasi-linear drop to zero, with slope  $\eta/h$ , where  $\eta$  is the viscosity of the glassy junction. The crossover velocity  $V^*$  is in practice much too small to be observable.

#### D. Sliding dynamics of a MCI :

##### 1. The Rice-Ruina friction law :

We can now sum up the above phenomenological analysis into a model of MCI dynamical friction which reads, with the help of equations (17), (22),(23) and ((29) :

$$F(\phi, \dot{x}) = \sigma_{s0} \Sigma_{r0} \left[ 1 + m \ln \left( 1 + \frac{\phi}{\tau} \right) \right] \left[ 1 + \alpha \ln \left( \frac{\dot{x}}{V_0} \right) \right] \quad (46)$$

$$\dot{\phi} = 1 - \frac{\dot{x}\phi}{D_0} \quad (47)$$

We saw that both  $m$  and  $\alpha$  are typically of order  $10^{-2}$ , so that it appears reasonable to neglect the  $m\alpha \ln^2$  term in expression (46) for the friction force. Moreover, we saw that the short time cutoff  $\tau$  associated with the early stage of area creep becomes relevant only for velocities  $\sim D_0/\tau$ , on the order of a few hundred  $\mu\text{m}/\text{sec}$  at least. For the moderately accelerated instationary dynamics which we will analyze below, in order of magnitude  $\phi \sim D_0/\dot{x}$  so that, in the low velocity regime considered here,  $\phi/\tau \ll 1$ . Equation (46) then reduces to the following expression for the dynamic friction coefficient :

$$\mu_d(\phi, \dot{x}) = \mu_d(V_0) + B \ln \left( \frac{\phi V_0}{D_0} \right) + A \ln \left( \frac{\dot{x}}{V_0} \right) \quad (48)$$

where the reference velocity  $V_0$  can be chosen at will in the above-mentioned velocity range. The constants  $B$  and  $A$  are defined in equations (19) and (30).

Equations (47) and (48) constitute the Rice-Ruina (RR) model, proposed by these authors in 1983 on the basis of Dieterich's experiments.

##### 2. The RR dynamics of a driven block :

The question then immediately arises of analyzing and testing experimentally the predictions of the model in terms of sliding dynamics. First of all, does it correctly describe the stick-slip (SS) oscillations of a driven block, and their disappearance at high enough stiffness?

Consider the system depicted on Figure 1. Let us assume for the moment that the sliding velocity is uniform along the interface (homogeneous sliding), i.e. that the block has a single degree of freedom, the position  $x(t)$  of e.g. its center of mass. Its equation of motion reads :

$$M\ddot{x} = -K(x - x_0(t)) - W\mu_d(\phi, \dot{x}) \quad (49)$$

where  $\mu_d$  and  $\phi$  are specified by equations (48) and (47), and  $(x - x_0(t))$  is the instantaneous elongation of the driving spring.

At any pulling velocity  $V$  there always exists a steady sliding solution, namely :

$$\dot{x} = V \quad \phi = \frac{D_0}{V} \quad x(t) - x_0(t) = \frac{W}{K} \mu_d \left( \frac{D_0}{V}, V \right) \quad (50)$$

In view of the non-linearities of the friction law, one must wonder about its dynamic stability, i.e. perform

a standard linear stability analysis : setting  $\dot{x} = V + \delta\dot{x}(t)$ ,  $\phi = D_0/V + \delta\phi(t)$ , one linearizes the dynamical equations in  $\delta\dot{x}$ ,  $\delta\phi$ . Thanks to the time invariance of the basic state, the solutions for them are of the form  $Const \exp(i\Omega t)$ . Steady sliding is stable (resp. unstable) when  $Im \Omega > 0$  (resp.  $< 0$ ).

This calculation is performed in Appendix C. It shows that, for given values of  $M$ ,  $W$  and  $V$ , steady motion is stable for  $K > K_c$ , with the critical stiffness given by:

$$K_c \frac{D_0}{W} = (\mu_\phi - \mu_{\dot{x}}) \left[ 1 + \frac{MV^2}{WD_0\mu_{\dot{x}}} \right] \quad (51)$$

At the bifurcation point ( $K = K_c$ )  $\Omega$  is pure real and has the value :

$$\Omega_c = \frac{V}{D_0} \sqrt{\frac{\mu_\phi - \mu_{\dot{x}}}{\mu_{\dot{x}}}} \quad (52)$$

That is, the corresponding bifurcation is of the Hopf type, signalling that for  $K \leq K_c$  motion should become oscillatory.

In equations (51), (52),  $\mu_\phi = \partial\mu_d/\partial(\ln\phi)$ ,  $\mu_{\dot{x}} = \partial\mu_d/\partial(\ln\dot{x})V$ , both derivatives being evaluated at  $\phi = D_0/V$ ,  $\dot{x} = V$ . The RR expression results in  $\mu_\phi = B$ ,  $\mu_{\dot{x}} = A$ . In the experiments aiming at characterizing the SS bifurcation, the block was sliding under its own weight :  $W = Mg$ . Then with  $D_0 \sim 1\mu\text{m}/\text{sec}$ ,  $A \sim 10^{-2}$ , the inertial correction in the second factor of the r.h.s. of equation (51) is of order  $10^{-5}(V_{\mu\text{m}/\text{s}})^2$ . So, inertia is negligible for  $V \lesssim 100\mu\text{m}/\text{sec}$ . Then the RR model predicts that the critical stiffness

$$K_c = (B - A) \frac{W}{D_0} \quad (53)$$

should be velocity-independent, while the critical pulsation

$$\Omega_c = \frac{V}{D_0} \sqrt{\frac{B - A}{A}} \quad (54)$$

The SS bifurcation has been studied on symmetric MCI involving paper [9], glassy PMMA and PS [29]. In these experiments,  $K$  was kept constant. Then, when  $M$  was increased at constant  $V$ , the initially steady motion was observed to bifurcate at a value  $(K/M)_c$  beyond which it develops oscillations whose amplitude grows continuously as  $K/M$  decreases, until true sticking phases appear (Figure 18). Tracking the bifurcation at various  $V$ 's leads to the stability diagram in the plane  $(K/M, V)$  of the control parameters, a typical example of which is displayed on Figure 19. It is seen that  $(K/M)_c$  is not strictly constant, but decreases slowly with increasing  $V$  at a rate on the order of 10 per cent per decade. On the other hand,  $V/\Omega_c$  was measured to be constant up to

experimental accuracy<sup>17</sup> [9]. So, the predictions of the RR model appear qualitatively satisfactory.

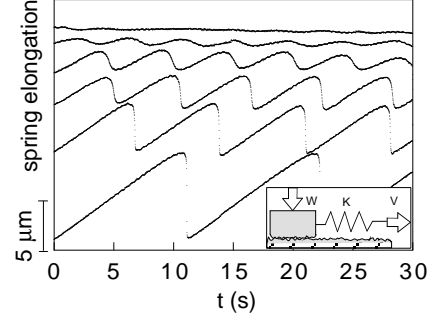


FIG. 18: Spring elongation (see inset) versus time for a paper/paper MCI pulled at the fixed velocity  $V = 1\mu\text{m}/\text{sec}$ . As  $K/W$  decreases, sliding motion bifurcates continuously from steady (upper curve) to periodic stick-slip of growing amplitude.

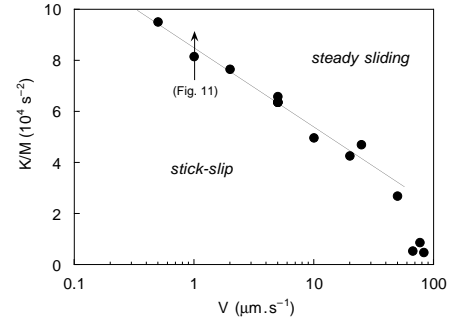


FIG. 19: Dynamic stability diagram of a PMMA/PMMA MCI in the low velocity range. Steady sliding is stable above the bifurcation curve  $(K/W)_c(V)$ .

The parameters  $A, B, D_0$  of the model are then evaluated as follows : measurements of  $d\mu_d/d(\ln V)$  yield  $(B - A)$ ,  $D_0$  is obtained by equation (53) from the value of  $(K/W)_c$  at some reference velocity – e.g.  $1\mu\text{m}/\text{sec}$  – then  $A$  is determined with the help of equation (54). For example, for a PMMA MCI, one thus obtains [50] :  $A = 1.2 \cdot 10^{-2} \pm 2 \cdot 10^{-3}$ ,  $B = 2.3 \cdot 10^{-2} \pm 2 \cdot 10^{-3}$ ,  $D_0 = 0.4 \pm 0.04\mu\text{m}$ . Such parameter values are fully compatible with those deduced from static aging and velocity jump experiments.

In order to test more thoroughly the validity of the phenomenological model, we have analyzed whether it

<sup>17</sup> The poor accuracy on  $\Omega_c$  was due in particular to the difficulty of extrapolating measurements necessarily performed at finite amplitude to the continuous bifurcation while, in this case, non linearities develop very fast [49].

correctly predicts a few other salient features of MCI block dynamics, among which :

(i) **Non-linear development of SS-like oscillations close to the bifurcation:** it must be mentioned first that the RR model as such (constant  $\mu_\phi = B$  and  $\mu_{\dot{x}} = A$ ) results in a highly singular behavior for  $K \leq K_c$  [51], namely unbounded growth of the velocity at finite time. This unphysical behavior, in contradiction with the observation of a continuous bifurcation, can be traced back to the simplifying assumption that  $\mu_\phi$  and  $\mu_{\dot{x}}$  are mere constants, which is also responsible for the fact that the model fails to account for the non zero slope of the  $K_c(V)$  bifurcation curve. Baumberger et al [49] relaxed this assumption by assigning the slope of  $K_c(V)$  to a  $(\ln^2 \phi)$  correction to expression (48) for the friction coefficient. A standard perturbation expansion then results<sup>18</sup>. This extension of the RR constitutive law accounted very satisfactorily for the growth of the oscillation amplitude and of the frequency shift with  $(K_c - K)$ .

(ii) **Creep-like sliding motion following cessation of the drive:** As can be seen on Figure 8 once the drive at velocity  $V$  is stopped, the block continues to slide while slowing down until it stops at a finite force level. Baumberger and Gauthier [52] analyzed the dependence of such relaxation curves on the control parameters  $K/W$ ,  $V$ . They showed that the RR model predicts that the total distance slipped before arrest should be  $V$ -independent, while experiments show a 100% increase on one decade of  $V$ . Again, this discrepancy is cured by including into equation (48) the same  $\ln^2 \phi$  correction as for non linear effects close to the bifurcation. An example of the resulting fit of relaxation data is shown on Figure 20.

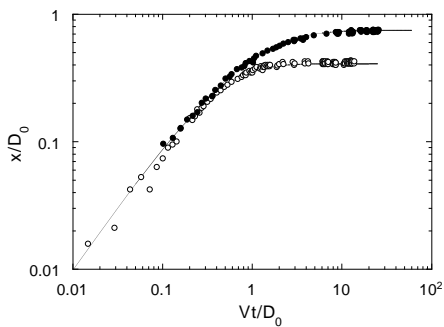


FIG. 20: Log-Log plot of reduced slip distance  $x/D_0$  vs reduced time  $Vt/D_0$  during creep-like relaxation of a paper/paper MCI. The system was sliding at  $V = 1\mu\text{m}/\text{sec}$  (open circles) and  $10\mu\text{m}/\text{sec}$  (full circles) until the drive was stopped at  $t = 0$ . The lines are the fits obtained from the RR model with a common set of parameters.

These two examples indicate the limits to be assigned to the rate and state model in its simplest version. While, clearly, the RR law does capture the essential features of MCI friction – namely geometric aging and dissipation governed by thermally-assisted mechanical instabilities on the nanometer scale – it is insufficient to account for finer dynamical features involving finite departures from stationary sliding. As described above, phenomenological corrections to the expression of  $\mu_d$  permit to extend the validity of the model. However, such extensions must be regarded with proper caution : clearly, the non-zero slope of the  $K_c(V)$  bifurcation curve indicates that an extension of expression (48) is needed. But this leaves open the question of the respective weights of the various possible corrections which we have mentioned when deriving expression (48). Not only is a  $\ln^2 \phi$  term possible, but also corrections of the form  $(\ln \dot{x})^2$  and  $(\ln \phi)(\ln \dot{x})$  as well as higher order ones. Moreover, corrections associated with the short age time cut-off  $\tau$  might become relevant. This would mean introducing many more parameters, in principle to be fitted from strongly non-linear dynamical features. As shown by the detailed analysis of the response to large amplitude normal force oscillations [53] [50], such fits become of more doubtful value as the dynamical complexity increases. This points towards the fact that formal extensions, or regularizations, of such a constitutive law, though they may appear useful, are in general difficult to legitimate in detail on a physical basis. So they must be considered with a critical eye when using them for predictive purposes.

### 3. Limitations of block models for extended MCI :

Seismic faults may be represented as spatially extended MCI under both normal and tangential loading. Studying their dynamics then means solving for the elastodynamic motion of two “semi-infinite” deformable media in frictional contact. It was the need for a realistic constitutive law for fault friction which motivated the work which resulted in the formulation of the RR model.

Once such a law is available, one is naturally led to plugging it into a continuum mechanics description. On the other hand, note that, since seismic events amount to the nucleation and propagation of interfacial cracks, they involve variations of deformation fields down to the very small scales relevant close to crack tips.

This leads us to an important remark resulting from the above analysis of the physics involved in the RR law. We saw that this law emerges from two averaging processes :

<sup>18</sup> The expansion parameter is found to be  $\epsilon \sim A/\mu_2$  with  $\mu_2 = [\partial^2 \mu_d / \partial (\ln x)^2]$ , so that for the RR model ( $\mu_2 = 0$ ) the expansion explodes. For PMMA,  $\mu_2$  is measured to be  $\sim 10^{-3}$ , hence  $\epsilon \sim 10$  : non linearities develop fast in the SS regime.

(i) the rheology described by the interfacial strength  $\sigma_s$  results from averaging over dissipative events involving nanometric regions within junctions; its expression is thus valid only on scales much above the nanometer one.

(ii) the creep growth of the real area of contact is translated into an geometric age which is an average over a large number of microcontacts. It thus only makes sense on a scale much larger than intercontact distances, i.e. typically millimetric.

As already mentioned, this makes the much discussed question of the ill-posedness [54] of the continuous limit a formal one. In view of the above remarks, which lead to the existence of a physically based small space scale cut-off, the most physical recipe for curing mathematical ill-posedness seems to be the one proposed by Simoes and Martins [55] : they wash out the UV singularity by replacing the local friction relation between interfacial normal and tangential stresses ( $\sigma_t(x) = -[\mu_d \sigma_n]_x$ ) by a non local one ( $\sigma_t(x) = -\int dx' w(x-x')[\mu_d \sigma_n]_{x'}$ ), with  $w$  a spreading function of finite width.

In practice, the dynamic complexity due to the nonlinearities of MCI friction [56] can only be studied numerically. This is implemented by discretizing the system into elastic blocks of size  $L \times L \times L$ <sup>19</sup>. Rice[57] has pointed out that the existence of the stick-slip instability imposes a natural upper limit on this block size. Indeed, such a discretization implies that the degrees of freedom of a block reduce to those of, say, its center of mass, internal ones being irrelevant. A block of size  $L$  has a tangential stiffness  $K_L \sim EL$ , with  $E$  an elastic modulus of the bulk. It bears the normal load  $W_L = \sigma_n L^2$ , with  $\sigma_n$  the average normal far field stress. It is stable against SS if  $K_L D_0 / W_L > (B - A)$ , i.e.  $L < L_R$  with :

$$L_R = \frac{E}{\sigma_n} \frac{1}{B - A} D_0 \quad (55)$$

Assume that a block has a size  $L_R < L < 2L_R$ . Cut it into 8 subblocks of size  $L/2$ . Each interfacial subblock is stable vis-à-vis SS, while the block is not. So the whole dynamic complexity on scale  $L$  is associated with the motion of the relative subblock position, which cannot therefore be considered irrelevant.

The maximum size of a discretization block is therefore  $L_R$ . From equation (55), with  $\sigma_n/E \sim 10^{-3}$ ,  $B - A \sim 10^{-2}$ ,  $D_0 \sim 1-10\mu\text{m}$ ,  $L_R$  lies in the meter range.

<sup>19</sup> Choosing blocks much longer in the transverse than in the longitudinal direction (i.e., in Burrige-Knopoff-like models, compressive stiffnesses much larger than shear ones) may lead to dynamical artefacts : for the so-called small events which involve only a few blocks, the associated elastic fields only affect depths, on the order of their lateral extent, much smaller than the block height. It is then illegitimate to neglect internal block degrees of freedom.

### III. JUNCTION RHEOLOGY : STRUCTURAL AGING/REJUVENATION EFFECTS

It is clear, at this stage, that the rough-on-rough MCI configuration only provides quite an indirect access to the analysis of junction rheology. Indeed, information about the interfacial strength  $\sigma_s$  can be extracted from friction data only after "deconvoluting" it from geometric aging effects, necessarily at the expense of precision. This might lead to overlooking finer physical features of dissipation within sheared junctions.

That such might indeed be the case emerged from the experimental study by Bureau et al [41] of the response of a rough/rough PMMA MCI to an oscillating shear force :

$$F(t) = F_0 + f \cos \omega t \quad (56)$$

biased about a value  $F_0$  below the static threshold. For very small  $f$ , the MCI responds elastically. As  $f$  is increased, the system enters a regime in which the oscillatory response is superimposed on a slow, self-decelerating, gross sliding motion which corresponds to a saturating, finite displacement. This regime prevails in a narrow amplitude range where  $F_{max} = F_0 + f \gtrsim F_s$ , where  $F_s$  is a static threshold. It was analyzed, on the basis of the RR model, as resulting essentially from the geometric age dynamics. During each force oscillation, the system alternates between sliding, hence rejuvenating, when  $F(t)$  is close below its maximum, and slowing down strongly, thus aging during the rest of the period. For  $f$  levels such that aging barely wins, gross motion decelerates and the system finally jams. Above a threshold  $f_{>}$ , rejuvenation wins, resulting in indefinite accelerated sliding.

The RR model accounts satisfactorily for the long time dynamics in the jamming regime. However, it exhibits, for small slid distances on the order of a few 100 nm, a clear discrepancy with experimental results which strongly suggests that another rejuvenation mechanism, distinct from the geometric one, hence ignored by the RR description, might be at work within the junctions.

#### A. Accessing junction rheology directly : suitable configurations

This confirms the interest of studying junction rheology directly, with the help of interfacial configurations which either are free of geometric aging or permit to circumvent this effect. This can be achieved in three different ways.

##### 1. Rough-on-flat multicontact interfaces

So far, we have restricted the definition of MCI to interfaces of macroscopic extent between two rough surfaces.

It is then tempting, in order to get direct information about junction rheology, to try and realize interfaces *à la* Greenwood which would not undergo the microcontact birth and death process responsible, for rough-on-rough systems, for the non trivial dependence of geometric age on the sliding dynamical history.

Such a configuration has been realized by Bureau et al [58] who studied friction between a rough PMMA slider (roughness  $\sim \mu\text{m}$ ) and a flat and smooth plate made of float glass (roughness  $\sim \text{nm}$ )<sup>20</sup>.

The interface is of the GW type but, due to translational invariance of the track, *the integrity of the contact population is now preserved upon sliding*. The load-bearing asperities creep as in a regular MCI but, since aging is not interrupted by sliding, the geometric age is simply the time  $T$  elapsed from the creation of the interface. The real area of contact  $\Sigma_r$  grows logarithmically with  $T$  so that, in steady motion at velocity  $V$ , the friction force  $F = \Sigma_r(\phi = T) \cdot \sigma_s(V)$ , becomes an increasing function of  $T$ , as can be seen on Figure 21. One can then take advantage of the slowing down of the logarithmic growth mode by letting the interface "mature" by waiting up to large  $T$ 's (typically 10 hours), then performing experiments during a comparatively short period (e.g.  $\lesssim 1$ hour) during which  $\Sigma_r$  remains quasi-constant, so that friction force variations are directly attributable to those of the interfacial strength  $\sigma_s$ .

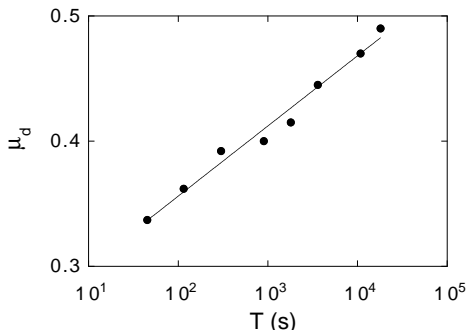


FIG. 21: Logarithmic growth of the *steady sliding* friction coefficient  $\mu_d$  at velocity  $V = 50\mu\text{m}/\text{sec}$  for a rough PMMA/flat glass MCI *vs* time  $T$  elapsed since the interface was created. Adapted from ref. [58].

## 2. Junctions in the Surface Force Apparatus

The surface force apparatus (SFA) was first developed [59] [60] to study adhesion. In a SFA, two atomically planar mica surfaces, slightly curved so as to realize a cross-cylinder geometry (Figure 22), are brought into contact

in the presence of a fluid (the lubricant). The interplate distance is decreased down to nanometric values on the order of a few molecular sizes. In this *boundary lubrication* regime where the fluid is very highly confined, the cylinders deform elastically, leading to a Hertz planar circular contact, with radius commonly in the  $10\mu\text{m}$  range.

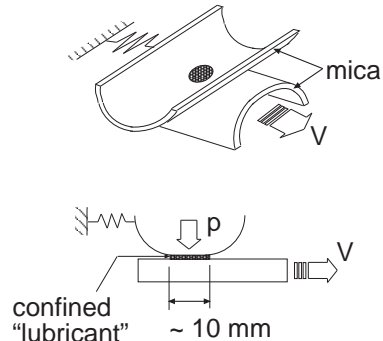


FIG. 22: The cross-cylinder geometry used in the SFA (upper sketch) is equivalent to a boundary lubricated sphere-plane contact (lower sketch).

The SFA was later modified [61] so as to allow for shear motion and measurement of friction forces. Since the area is measured optically, the normal stress borne by the contact is directly accessible, as well as the shear stress associated with frictional dissipation in the *junction formed by the lubricant*. In many instances (see below) such boundary lubrication layers behave as weak disordered solids, exhibiting an elastic regime at low shear levels.

## 3. Extended soft contacts

We refer here to the contacts which form between a highly compliant (soft) slider with a smooth surface and a hard flat smooth track. High slider compliance ensures that molecular adhesive contact is realized everywhere along the interface, even in the presence of submillimetric roughness.

Such contacts can be achieved in either of two configurations :

— *flat-on-flat*: up to now, this geometry has been used with sliders made of moulded hydrogels (Young moduli in the 1 – 10 kPa range) [62] [63]. The contact lateral extent is usually of order centimeters.

— *ball-on-flat*: this is the configuration commonly used to study friction at elastomer/glass interfaces [64] [65] [66]. Pressing the ball onto the flat under controlled normal load results in the formation of a circular adhesive Hertz contact [13]. Since elastomer Young moduli typically lie in the 1 – 10 MPa range, contact radii in such experiments are commonly of order millimeters.

<sup>20</sup> Since glass is much harder than PMMA, no ploughing of the track by the slider asperities takes place.

## B. MCI junctions revisited :

The results described here were obtained by Bureau et al [58] on MCI formed by rough PMMA sliding on smooth (float) glass. The surface state of the glass was controlled by grafting onto it a single monolayer of short silane molecules, which passivate strongly adhesive sites.

As already mentioned, such interfaces, when “old enough”, can be considered to work at constant area of contact  $\Sigma_r$ , thus giving direct access to variations of the frictional stress <sup>21</sup>.

### 1. Structural aging :

The central result is illustrated on Figure 23. Namely, standard stop-and-go experiments (see §II.B.1) reveal the presence of a static friction peak, the amplitude of which grows logarithmically with the waiting time  $t_w$  (Figure 24).

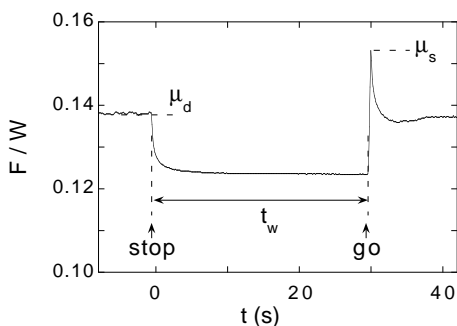


FIG. 23: Reduced shear force on a rough PMMA/silanized flat glass MCI in a stop and go experiment. For  $t < 0$  the block slides steadily ( $V = 10\mu\text{m}/\text{sec}$ ). After the drive is stopped ( $t = 0$ ) the slider slows down and stops at a self-selected stress level. At  $t = 30$  s loading is resumed at the initial velocity. Adapted from [58].

Contrary to what is the case for rough/rough MCI, this peak cannot be associated with geometric aging, which is not operative here. On the other hand, the very existence of a  $\mu_s(t_w)$  larger than the dynamic  $\mu_d$  means that the interface is the seat of an aging-when-waiting *vs* rejuvenating-when-sliding process, which must therefore necessarily take place within the junctions and affect their structure. The existence of this *structural aging* entails that  $\sigma_s$  is not, as we assumed up to now, a mere function of the instantaneous sliding velocity  $\dot{x}$ , but does itself depend upon the dynamical history of the interface.

Moreover, one observes that the structural aging rate depends noticeably on the value of the tangential stress applied during the stop phase (see Figure 24) : the lower its level, the slower aging is (see figure 5 of reference [58]).

Finally, in many cases – and especially for small waiting stresses – structural aging becomes observable only after a finite, strongly sample-dependent, *latency time*  $\tau_L$ .

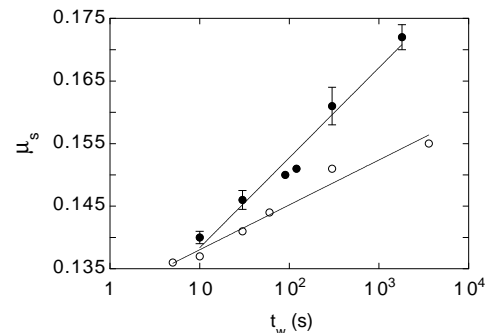


FIG. 24: Logarithmic growth of the static friction coefficient  $\mu_s$  with waiting time  $t_w$ . Aging at rest under : (●) the self-selected arrest shear stress; (○) null stress. From reference [58].

### 2. Steady sliding dynamic friction :

Figure 25 shows a typical example of the velocity dependence observed for  $\mu_d$ . It exhibits a minimum at  $V = V_{min}$ . The velocity-weakening observed for  $V < V_{min}$  provides another evidence that the structural age decreases with  $V$ , i.e. that sliding induces rejuvenation.

For  $V > V_{min}$ ,  $\mu_d$  increases quasi-logarithmically ( $\mu_d/\mu_{min} \approx (1 + \alpha \ln(V/V_{min}))$ ). That is, we recover here the expression of  $\sigma_s$  (equation (29)) deduced from the analysis of experiments on rough/rough MCI, which were used to formulate the RR model. Moreover, the reduced slope  $\alpha \simeq 4.10^{-2}$  has a magnitude comparable with the value ( $\alpha \simeq 5.10^{-2}$ ) found for rough/rough PMMA junctions. This enables us to conclude that already quite close above  $V_{min}$ , the rejuvenation effect is quasi-saturated.

### 3. Discussion

This phenomenology, the fine details of which were masked, for rough/rough systems, by the larger effects of geometric aging <sup>22</sup>, appears qualitatively consistent with

<sup>21</sup> As the absolute value of  $\Sigma_r$  is not measurable accurately, the absolute value of  $\sigma_s$  cannot be accessed in this configuration.

<sup>22</sup> As can be seen on Figure 24, the log-slope of  $\mu_s$  associated with structural aging is on the order of a few  $10^{-3}$ , typically from 10

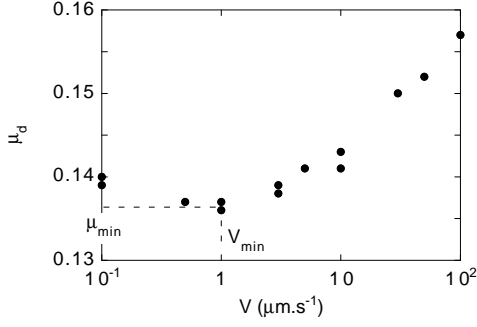


FIG. 25: Dynamic friction coefficient  $\mu_d$  vs velocity  $V$ . From reference [58].

our description of junctions as confined weak glassy media. Indeed, it is closely akin to the behavior of sheared bulk soft glassy materials, such as colloidal glasses [67] [68] and pastes [69]. The rheology of these systems has also been modeled [48] [70] [71] as resulting from the interplay between :

- aging at rest, i.e. strengthening via slow relaxation down the highly multistable energy landscape characteristic of quenched disordered, jammed, media.

- rejuvenation by motion, which can be seen as reshuffling the populations of the local minima.

In the sliding (i.e. plastic) regime, the rate of the localized dissipative events invoked in §II.C.4 should be increased by the decrease of the energy barriers due to stress induced biasing. The “young”, shallow energy states which were depopulated as aging pushed the system into “older”, deeper ones, thus can get repopulated : the sheared soft glass rejuvenates.

In the same perspective, one may tentatively interpret the above-mentioned dependence of the aging rate on waiting stress level as follows. In a stop-and-go experiment, the “stop” acts as a mechanical quench of the strongly rejuvenated formerly sliding state. Aging then restarts in a landscape with barriers whose height is decreased by stress-induced biasing, hence accelerates when the stress level increases <sup>23</sup>.

to 4 times smaller than the aging slopes for rough/rough MCI. This leads one to conclude that, in the latter case, the growth of  $\mu_s$ , though dominated by the geometric effect, does contain a small contribution due to structural aging.

<sup>23</sup> Viasnoff and Lequeux [72] have found that applying to a colloidal glass, aging under stress-free conditions, an oscillating shear stress of finite duration does result in a strong perturbation of the aging process. However, it is important to note that, in their experiment, the stress amplitude is larger than the yield stress of the material, which certainly results in some non-stationary flow. This contrasts with the situation of ref. [58], where the applied waiting stress does not provoke any sliding.

## C. Boundary Lubrication Junctions

Over the past twenty years a considerable body of results has come out of friction experiments performed in the SFA, in the boundary lubrication (BL) regime. It is much too vast to be extensively reviewed here. We limit ourselves to those salient features which we consider to be most relevant in the perspective of this article.

### 1. Confinement-induced solidification

When the “lubricant” – a liquid in the bulk phase at the temperature of the experiment – is compressed between the two mica surfaces, it is gradually squeezed out until its thickness is reduced to a few molecular sizes. Then, for materials composed of small, spherical or short-chain, molecules (e.g. OMCTS – an inert silicone – squalane, linear alkanes) one observes [61] that the normal force-*vs*-thickness  $F_N(D)$  curve develops oscillations whose amplitude grows rapidly as  $D$  decreases (see Figure 26). This behavior can be ascribed to the layering of the confined fluid, each successive minimum being reached by squeezing out one more full layer.

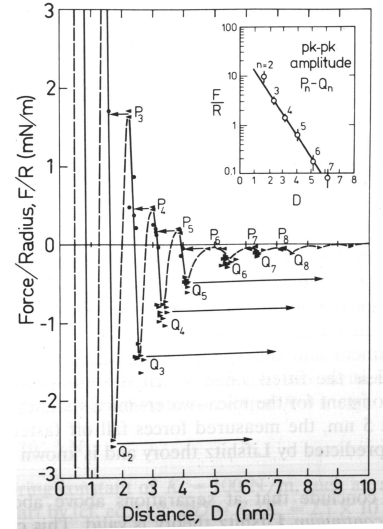


FIG. 26: Measured oscillatory force between two mica surfaces immersed in the liquid OMCTS. The arrows indicate inward or outward jumps from unstable to stable positions. Inset : peak-to-peak amplitudes of the oscillations as a function of  $D$ . From ref. [61].

Thin enough (typically 3–4 molecular layers) such junctions, when sheared, exhibit an elastic response at low shear stress levels, until they reach a static threshold where they yield and start sliding [73] [74] [75]. This demonstrates that they have solidified under the effect of

the high confinement <sup>24</sup>. This behavior has been confirmed by numerical studies [76].

Klein and Kumacheva [77] found that, in the case of OMCTS (and at variance with previous results reported in [75]), the liquid-to-solid transition occurs abruptly when decreasing the number of layers from 7 to 6. Whether or not such abruptness is a general feature has not been documented on different systems.

Finally, it was shown in [74] that increasing the temperature makes the confined solid weaker, i.e. leads to a decrease of its yield stress.

It is important to note that the highest normal stresses which can be realized in the SFA are on the order of 10 MPa. That is, they are at least one order of magnitude smaller than the levels met in MCI microcontacts, which we have seen to be comparable with the yield stress of the confining bulk solids.

## 2. Structural aging

Stop and go experiments show that the static threshold of solidified BL junctions increases with the waiting time  $t_w$  spent at rest. This strengthening, which reveals structural aging, has been studied quantitatively on a variety of lubricants, including hexadecane [74], squalane [78] [79] and a star-shaped polymer melt [80]. Strengthening also manifests itself through the increase with  $t_w$  of the layer elastic stiffness [81].

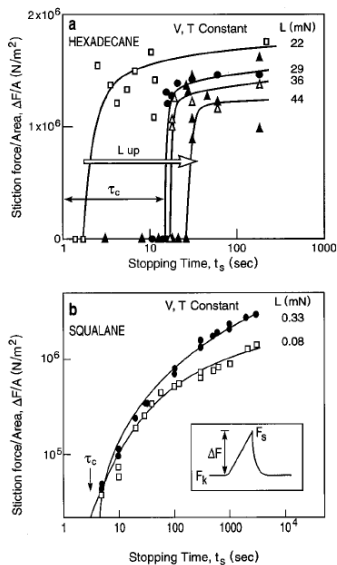


FIG. 27: Stiction peak heights *vs* waiting time  $t_s$  for (a) hexadecane (from ref. [74]); (b) squalane (from ref. [82]).  $L$  is the normal load,  $\tau_c$  the latency time.

In all cases, strengthening is slow, namely either linear on a logarithmic  $t_w$ -scale [74] [81] or somewhat faster [79]. As illustrated on figure 27, finite latency times, ranging up to about 10 seconds, previous to aging, have been observed on hexadecane [74] and several lubricants including squalane [78]. This result was later contradicted, for squalane, in reference [79] – a discrepancy which is possibly ascribable to the difficulty of defining such a notion with high precision. Indeed, at short waiting times, the height of the stiction peak (the difference between the static threshold force and the dynamic one at the imposed driving velocity) becomes very small. Since accuracy is limited by the noise level, it may be difficult to ascertain whether one should invoke complete latency or a gradual increase of the aging rate.

Finally, Drummond and Israelachvili [78] have compared, for squalane and a star-shaped lubricant (PAO), aging under zero and a finite shear stress close below the dynamic level. Contrary to what was observed on PMMA/glass MCI, they find that, for a given  $t_w$ , the stiction peak is systematically higher when waiting under zero shear stress. This leads the authors to associate rejuvenation upon sliding, responsible for the force drop producing the stiction peak, with shear-induced molecular alignment, whose relaxation is certainly faster at zero waiting stress. We will come back to this in the discussion of §III.F.

## 3. Sliding dynamics

All BL systems with a finite static threshold exhibit the same dynamical behavior in the explored low driving velocity domain (ranging from  $\lesssim 10^{-2} \mu\text{m}/\text{sec}$  to a few  $10 \mu\text{m}/\text{sec}$ ). Namely, as illustrated by figure 28 :

- For  $V < V_{c1}$  periodic stick-slip (SS) motion.
- In a finite range  $V_{c1} < V < V_{c2}$ , the motion exhibits intermittency, in the form of randomly spaced stick-slip peaks [82].
- For  $V > V_{c2}$ , these peaks disappear, sliding becomes steady [82] and, in this regime, dynamic friction is  $V$ -weakening.

In most cases studied, the amplitude of the SS force signal is roughly constant up to  $V_{c2}$  <sup>25</sup>.

It is worth mentioning that a qualitatively similar behavior is observed with gelatin/glass extended sliding contacts [83]. In this latter case it is associated with the fact that, in the SS regime, sliding is spatially inhomogeneous – it occurs via propagating slip pulses (see

<sup>24</sup> For some fluids made of short-chain molecules, e.g. hexadecane [74], the solid-like response only builds up after a finite amount of shear-induced sliding – suggesting that in this case initial sliding helps ordering.

<sup>25</sup> Whether or not such a discontinuous transition exhibits hysteresis upon increasing/decreasing  $V$  is not documented, to our knowledge.



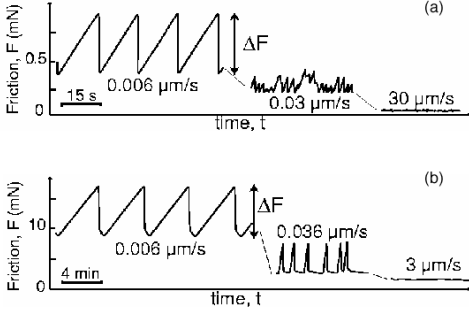


FIG. 28: Dynamic friction force *vs* time for a squalane boundary lubrication layer driven at increasing velocities under pressures  $P = 1.4$  MPa (a); 5.4 MPa (b) (adapted from Figure 2 of ref. [79]).

§III.C.4 below). In the intermittent regime above  $V_{c1}$ , the corresponding large force peaks are interspersed with smaller ones due to nucleation, propagation and death of small slip events within the contact. This remark suggests the possibility that sliding in BL junctions might also exhibit spatial complexity. Such a model has been proposed by Persson [3], who invokes the nucleation and propagation of “shear-melted islands”.

In an extensive study of squalane junctions, Gourdon and Israelachvili [79] have, in particular, investigated the effect of normal load on the sliding dynamics. They find that the dynamics described above prevails at high normal stresses ( $P \gtrsim 5$  MPa). However, at lower normal stresses ( $\lesssim 2$  MPa), a different behavior is observed: for  $V \gtrsim V_{c1}$ , the amplitude of the erratic stick-slip decreases continuously down to zero.

Finally, using a SFA with a large sliding range ( $500\mu\text{m}$ ), Drummond and Israelachvili [78] have studied, for squalane, the shape of friction force transients following velocity jumps. These transients are long-lived, and characterized by a distance comparable with the contact diameter.

#### D. Extended Soft Contacts : Gelatin/Glass Friction

They are particularly easy to realize with hydrogels, such as gelatin, which exhibit both ultra-low shear moduli (typically a few kPa) and an extended elastic regime. Their high solvent content (typically  $\gtrsim 80\%$ ) endows them with specific frictional properties resulting from their poroelastic character [84]. For this reason, we separate this case from that of non-swollen elastomers.

Gong and Osada [62] have performed extensive studies of :

- the influence on the dynamic friction level of the (attractive *vs* repulsive) nature of gel/substrate interactions. They have shown that repulsive interactions re-

sult in the formation of a thin interfacial layer of solvent, hence to hydrodynamic lubrication. For attractive couples, friction is strongly influenced by the formation of transient adhesive polymer-substrate bonds, which they modeled by adapting a description due to Schallamach (see below).

- the dependence of the friction force on normal loads in these different situations.

However, up to now, the only system on which the nature of the sliding dynamics has been fully analyzed is gelatin on glass [63], on which we now concentrate.

##### 1. Static threshold

The experiments described here were performed under zero normal load, adhesion being strong enough to lead to solid friction, i.e. to a finite static threshold.

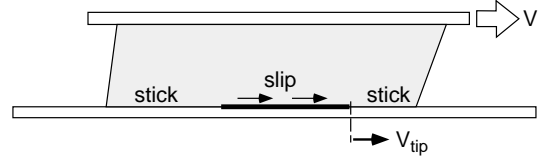


FIG. 29: Schematic representation of a gel block driven at velocity  $V > V_c$  (see text). The self-healing slip pulse propagates at velocity  $V_{tip}$ .

When a gelatin block is sheared (Figure 29), as the force increases, the gel/glass contact first remains pinned, and the block deforms elastically. At a threshold stress  $\sigma_0$  sliding sets in. This occurs via nucleation at the trailing block edge of an interfacial fracture without measurable vertical opening, which propagates forward with a constant velocity  $V_{tip}$  in the mm-cm/sec range, i.e. much smaller than that of transverse sound (typically  $\sim 1$  m/sec)<sup>26</sup>. By changing the gelatin concentration, hence the mesh size  $\xi$ , and the solvent viscosity  $\eta_s$ , it appears that  $V_{tip} \sim D/\xi$ , with  $D$  the collective diffusion coefficient [84], measured from quasi-elastic light scattering experiments [85] :  $D \sim G\xi^2/\eta_s \sim k_B T/\eta_s \xi$ , with  $G \sim k_B T/\xi^3$  the shear modulus.

This indicates that the interfacial pinning, which must be severed in order to crack, is provided by bonds with a typical lateral spacing  $d$  on the order of the mesh size.

Indeed, the value of the self-selected  $V_{tip}$  can be interpreted as follows. The energy released by bond snapping events is emitted at the frequency  $\omega \sim V_{tip}/d$ , and wave vector  $q \sim d^{-1}$ . The lowest deformation mode of the gel block is the so-called Biot mode, associated with network diffusion within the solvent  $\omega_D = Dq^2$ . It resonates with

<sup>26</sup> Note that, while the shear modulus is controlled by the elasticity of the loose polymer network, the undrained bulk modulus is that of the solvent, so hydrogels can be considered incompressible.

emission, hence becomes most efficient to dissipate the fracture energy, when  $\omega_D \sim \omega$ , from which it emerges that  $d \sim \xi$ <sup>27</sup>.

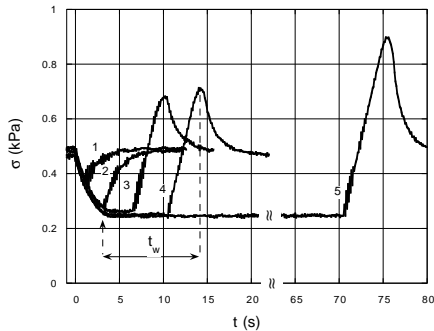


FIG. 30: Aging-induced growth of the static friction peak (curves 3, 4, 5) for a 5% gelatin gel/glass interface. If the drive is resumed before the interface resticks (left of vertical arrow) no peak is observed (curves 1, 2). From ref. [63].

Now, one also observes, as shown on figure 30, that the threshold  $\sigma_0$  for crack nucleation is not a constant, but increases logarithmically with waiting time at rest  $t_w$  (in the explored range  $t_w \gtrsim 1\text{sec}$ ). This indicates that adhesive bonding between the substrate and the polymer tails and/or loops dangling from the disordered network proceeds on two time scales : a rather fast one, which leads to finite static pinning with a bond areal density  $\sim \xi^2$ , followed by a slow, thermally activated relaxation of the adsorbed polymer configurations leading to the slow increase of this density.

## 2. Sliding dynamics

When the gel block is driven at velocity  $V$ , two types of dynamics are observed.

(i) Above a critical velocity  $V_c$  (ranging, depending on gel composition, from  $\sim 25$  to  $\sim 250\mu\text{m}/\text{sec}$ ), sliding is steady. The sliding stress  $\sigma_s(V)$  is velocity-strengthening, and corresponds to a shear-thinning rheology, namely :

$$\sigma_s(V) \sim V^{1-\alpha}$$

with  $\alpha = 0.6 \pm 0.07$ . This is reminiscent of the behavior of polymer solutions [87], and suggests that, in this sliding regime, interfacial pinning plays only a minor role,

dissipation being due to the viscosity of a layer of thickness the mesh size (on the order of 10 nm) formed by a solution of polymer segments attached to the network. If such is the case, the shear strain rate  $\dot{\gamma} \sim V/\xi$ , and the effective viscosity

$$\eta_{eff} = \frac{\sigma_s}{\dot{\gamma}} \sim \eta_s (\dot{\gamma} \tau_R)^{-\alpha}$$

with  $\tau_R$  a typical relaxation time for a chain length  $\sim \xi$  in solution. Using for  $\tau_R$  the Rouse time one gets, for a variety of gelatin concentrations and solvent viscosities, the collapse of data shown on Figure 31, which lends excellent support to the above interpretation.

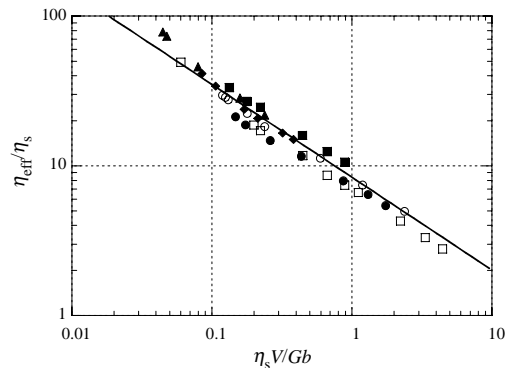


FIG. 31: Reduced effective viscosity  $\eta_{eff}/\eta_s$  versus Weissenberg number  $We = \dot{\gamma} \tau_R$  for gelatin gels in water/glycerol solvents. Filled symbols : gelatin (wt %) 5(circles), 8 (squares), 10 (triangles), 15 (diamonds) in pure water. Open symbols: 5 wt % gelatin in 21 % (circles) and 42 % (squares) glycerol in water.

(ii) For  $V < V_c$ , periodic stick-slip prevails. Optical observation shows that during the “slip phase” sliding is not homogeneous, but proceeds by propagation of *self-healing pulses* (Figure 29). Pulse heads are the previously described crack tips, behind which the local slip velocity  $v$  decreases from the standard quasi-diverging field towards the driving value  $V$ . However, this regular decrease is suddenly interrupted when  $v$  reaches a value equal to the critical value  $V_c$  which turns out to coincide with the upper limit of the stick-slip regime. At  $v = V_c$ , resticking (healing) occurs quasi-discontinuously.

When  $V$  approaches  $V_c$  from below, the pulse length increases, so that the transition to steady sliding takes place via increasing time spacing of pulses of quasi-constant amplitude, while being non hysteretic. Moreover, for  $V \simeq V_c$ , an intermittent behavior, already described above (§III.C.3) is observed – the interpulse spacing becomes erratic, and they are interspeded with smaller force signals associated to short-lived small propagating slip events. A more detailed characterization of this complex dynamical behavior will certainly be of interest.

<sup>27</sup> It is worth mentioning that Rubinstein et al [86] have recently observed that sliding between purely elastic solids also sets in via propagation of interfacial cracks, but in the elastic case these propagate at velocities in the sonic range. The low values of  $V_{tip}$  for gelatin are therefore, in contrast, a signature of poroelasticity.

### 3. Rate and state interpretation

Clearly, as for the previously considered cases, static strengthening means interfacial aging at rest, which we expect to be associated with rejuvenation, i.e. weakening, upon sliding, as proved by the reproducibility of  $\sigma_0(t_w)$  in stop and go experiments.

This is consistent with the abruptness of the resticking process at the trailing edge of the self-healing pulses. Indeed, assume that the steady-sliding characteristics is  $V$ -weakening for  $V < V_{min}$ . Close behind the pulse head, the local  $v$ , larger than  $V_{min}$ , lies on the locally stable branch of  $\sigma_s(V)$ . As the distance behind the head increases,  $v$  decreases. When it reaches  $V_{min}$ , the interface becomes unstable on a small spatial scale (smaller than the optical resolution). In other words, since the driving stiffness, provided by the very compliant gel block, is extremely low, the interface jumps down to  $V = 0$  at quasi-constant stress. This leads to concluding that the resticking velocity  $V_c$  corresponds to a minimum of  $\sigma_s(V)$  above which, as appeared in the previous paragraph, interfacial pinning should be negligible. This interpretation is also consistent with the coincidence of the resticking velocity and the disappearance of stick-slip as soon as the asymptotic value  $V$  of the local velocity  $v$ , needed for steady sliding to get established, reaches the stable branch of  $\sigma_s(V)$ .

So, here again, it seems natural to try and define a structural age of the gel/glass interface. Quite clearly, the corresponding dynamic state variable must somehow measure the pinning energy associated with the formation of polymer-glass adhesive bonds.

Already 50 years ago, Schallamach [64] proposed, in the context of dry rubber friction, a seminal model of such a dynamic state variable, which remains the basis of all more recent theories of gel [62] and rubber [88] [89] friction. In this model, briefly summarized an discussed in Appendix D, the elementary mechanical instability (see §II.C.4) is the snapping of a bonded molecule out of its adsorption site under shear loading through an elastic spring (here the polymer segment). Once this energy barrier has been jumped over, under the combined effect of loading and thermal activation, the molecule is freely advected until it readsorbs via a thermally activated process. Of course, readsorption is thwarted by advection, which limits the time available for this process to take place. The state variable is thus the density of bonded molecules. The friction stress is the product of this  $V$ -weakening density, and of the  $V$ -strengthening average depinning force (the faster advection, the less time for escaping above high barriers). So it exhibits a bell shape with a maximum at  $V = V_{max}$ . The low velocity regime is an Eyring viscous one, with the bond density close to its equilibrium saturation level. In the  $V$ -weakening high velocity regime the depinning force saturates,  $\sigma_s(V)$  is then fully controlled by dynamic rejuvenation, hence vanishes for  $V \rightarrow \infty$ .

Models of the Schallamach type call for two important

remarks :

(i) The extent of the Eyring-like low  $V$  regime ( $V < \tilde{V}$ , see Figure 35) crucially depends on the height of the desorption barrier. When, as often assumed – explicitly or not – it is on the order of a few  $k_B T$ ,  $\tilde{V}$  is non-negligible. A strong consequence is that, in such cases, no static threshold should be observable except if one could load at exceedingly large velocities. This points towards the interest of systematically associating studies of dynamic friction in such systems with stop and go experiments.

Gelatin/glass interfaces exhibit well defined static force peaks and crack tips. We must therefore conclude that, in this case, we are dealing with strong bonds – in which case  $\tilde{V}$  becomes negligibly small (see end of §II.C.4).

(ii) If we stick to the Schallamach prediction, in the case of gelatin,  $\sigma_s(V)$  should be uniformly  $V$ -weakening, since in the explored range  $V \gg V_{max}$ . How can one then explain the existence of the  $V > V_c$  strengthening behavior?

We meet here with an important shortcoming of the Schallamach model. Namely, unpinned molecules are assumed to glide freely, that is, viscous dissipation in the interfacial layer is omitted – although, since its thickness is typically nanometric, shear rate levels are high. In the case of gelatin we saw that, on the contrary, it is this contribution which fully accounts for the observed non-newtonian friction at the essentially depinned interface. This illustrates the importance of taking into account in this kind of problem, not only interfacial pinning, but, as well, junction viscosity. When both effects are of comparable importance, this open problem becomes a true nanofluidics one, as far as the size of the confined polymer chains is precisely comparable with the thickness of the “channel”, i.e. the junction.

In summary, once complemented with standard viscous dissipation in the sliding junction, the Schallamach picture, which identifies the state variable with the density of adsorbed bonds, provides a sound basis on which to modelize gel friction. Clearly, a more elaborate modelization of the dangling chains, taking into account the existence of a multiplicity of possible bonding configurations [90] and a detailed description of chain dynamics [88] would be needed to make such models more quantitative, as well as to touch upon the question of long term aging.

### E. Extended Soft Contacts : Dry Elastomer Friction

Due to its importance in a number of applied fields (e.g., to name only a few, traction of tires, windshield wiper efficiency and durability), this question has been a subject of very active investigation in the past six decades. We restrict ourselves here to a sketchy summary of the commonly accepted concepts used for interpretation of interface geometry *vs* molecular adhesion effects. For extensive bibliographies, see [91] [92] [66].

We consider here the case of elastomers in extended contact with much stiffer solids, which can thus be assumed non deformable. Bulk viscoelastic dissipation is very important in rubbers. Its strong temperature dependence follows the so-called WLF time-temperature superposition principle [93]. Grosch [94], and Ludema and Tabor [95], have shown that one must distinguish between contributions to the sliding friction stress governed respectively by bulk and interfacial dissipation.

### 1. Bulk dissipation

It comes into play as soon as the stiff partner surface exhibits non negligible roughness - on a scale larger than the average cross-link spacing. Assume for a moment that the roughness has a characteristic wavelength  $\lambda$ . Then, in stationary sliding, a given material point within the elastomer feels a stress field modulated at a frequency  $\omega \sim V/\lambda$ , which penetrates down to a depth  $\sim \lambda$  below the surface. This results in a dissipation governed by the loss modulus of the bulk,  $G''(\omega)$ , i.e. obeying a  $V - T$  superposition principle. One is thus able to account for the most salient feature of rubber friction, namely the existence of a maximum of the  $\sigma_s(V)$  curve, at a velocity  $V_m$ , which increases with the temperature  $T$ , above which stick-slip motion sets in [94].

### 2. Interfacial dissipation

Grosch [94] identified, in his experimental results on friction of several elastomers on silicon carbide paper, an additional feature - a shoulder on the  $\sigma_s(V)$  curve at a velocity  $V_m \simeq \omega_m \Lambda$ , where  $\omega_m$  corresponds to the maximum of the loss modulus and  $\Lambda \sim 6\text{nm}$ . This shoulder turned into a broad maximum when sliding on smooth “wavy” glass. He attributed this to interfacial dissipation - i.e. to the snapping out of advected adhesive bonds as modeled by Schallamach (see §III.D.3).

It is only recently that progress in surface control enabled Vorvolakos and Chaudhury (VC) [66] to reconsider this question. They used two model systems, constituted of cross-linked PDMS sliding on (i) a self-assembled silane monolayer supported by a Si wafer (ii) a thin film of glassy PS. They were thus able to get rid of surface roughness effects, hence of bulk dissipation.

Silane coverage results in very low energy surfaces, so one expects polymer substrate adhesive bonds to be rather weak in this case and, hence, Schallamach’s model to be appropriate. Indeed, VC show that their results for  $\sigma_s(V)$  in this system (see figure 32), which extend over 5 velocity decades, are well explained qualitatively in this frame<sup>28</sup>. Moreover, they deduce from a time-

temperature superposition argument an energy scale  $\sim 25 \text{kJ}\cdot\text{mol}^{-1}$ , i.e.  $\sim 0.3 \text{eV}/\text{bond}$ . Whether this energy, much larger than the van der Waals ones expected for PDMS/silane interactions, is relevant to adhesive bond snapping in this system remains an open question.

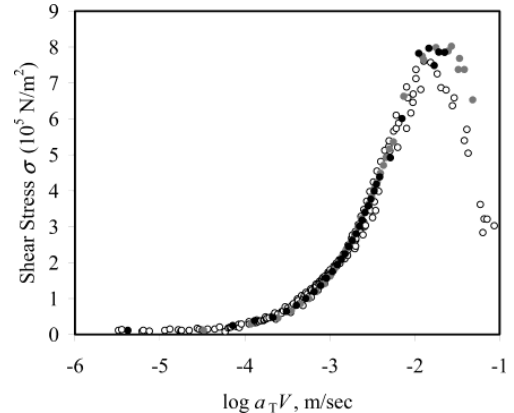


FIG. 32: Temperature-dependent friction stress data for PDMS on a silanized silicon surface shifted to room temperature using a WLF shift factor. Open, gray and black circles represent data at 298, 318 and 348 K respectively. From ref. [66].

PDMS bonding to PS is likely to be stronger than that on silane. Indeed, consideration of the VC results in the low velocity limit leads to raising the question of the possible existence of a finite static friction threshold. Systematic investigation of the transient behavior at the onset of sliding would certainly be enlightening.

Finally, it is worth mentioning that non homogeneous sliding has been observed [96] [91] at some smooth soft rubber/glass interfaces. This occurs via propagating self healing pulses. But, contrary to the gelatin case where contact is maintained in the sliding regions, these *Schallamach waves* are of the mode-I fracture type. That is, they consist of regions of interfacial detachment with macroscopic opening which re-adhere at the back edge. So, in this regime, dissipation is essentially controlled by adhesion hysteresis [65]. Though high compliance and large viscoelastic losses are thought to promote this sliding mode, no prediction relating material properties to the dynamics, nor even to the occurrence of Schallamach waves is available up to now.

As already mentioned, it should come into play, especially in the  $V$ -weakening regime  $V > V_m$ , where it is certainly needed to interpret the observed stick-slip behavior.

<sup>28</sup> Interfacial viscous dissipation is neglected in the VC analysis.

### F. A tentative classification : Jammed junction plasticity vs adsorption controlled dynamics

The various frictional behaviors briefly described above pertain to junctions which differ in several respects, namely :

- Normal stress level, i.e. confinement pressure  $P$ , which ranges from zero (gelatin) to about the yield stress of the softer bulk material (rough on flat MCI).
- Level of adhesive interactions, i.e. strength of the pinning sites provided by the confining potential. This ranges from very weak (fully silanized substrates) to strong (e.g. bare glass).
- Density of adsorbable units, ranging from dense (polymer glasses) to (semi)dilute (hydrogels).

All these systems share two properties :

- they exhibit a static threshold <sup>29</sup>
- this threshold ages slowly with time spent at rest.

The experimental signature of this structural aging is the slow (in general quasi-logarithmic) growth of the upper limit of the elastic regime. In experiments where the slider is remotely driven at constant velocity  $V$ , it results in general in a force peak. This unambiguously reveals rejuvenation upon sliding, since the sliding velocity  $v$  is equal to the driving one  $V$  both in the steady sliding state and at the peak, where the slid distance is minute, so that the age is basically given by the waiting time before pulling <sup>30</sup>. This means that the state of the sliding junction is specified, not only by its instantaneous velocity, i.e. by the shear rate  $\dot{\gamma}$  it experiences, but also by the value of some dynamical state variable.

On the other hand, different classes of systems exhibit different steady state rheologies, from logarithmic strengthening for highly confined PMMA/glass to power law for gelatin.

While these behaviors call for rate and state descriptions, it is clear that various classes of systems must be distinguished, in terms of the microscopic nature of the state variable  $\varphi$ , which is necessarily related with the junction structure and, hence, with the pinning mechanism giving rise to static friction. The existing body of experimental results discussed in §III.B–E is still far from sufficient to provide a firm basis for such a phenomenology. So, the classification which we propose here is only tentative, and primarily intended to help structuring further questions to be, in a first stage, investigated experimentally.

Let us start from the very high confinement regime, realized in the MCI configuration (§III.B) where, for

PMMA, the confining pressure  $P \sim 100$  MPa is comparable with the bulk yield stress. We saw that junctions between such a polymer glass and highly silanized glass behave as soft glassy nanometer-thick media.

In other words, we claim that, in such a case, the disordered material of the dense junction jams [8], i.e. solidifies under confinement. It ages as a glass, by relaxing towards deeper local minima of the energy landscape (inherent states) and, when it flows, dissipation can be attributed to irreversible flips of molecular-sized shear transformation zones (STZ) [44]. In this case, *frictional sliding is nothing but plastic flow of this interfacial glass* which, being weaker than the bulk, naturally localizes shear.

Now, note that, in the MCI experiments, when the glass substrate is well silanized, no direct manifestation of the polymeric nature of the junctions is observed. However, when the same experiments are performed on a poorly silanized substrate [58], the previously observed rather narrow aging peak persists, but is followed by a long bumpy stress transient (see Figure 33). Moreover if, after reaching the steady state, one performs stop-and-go tests with a high stopping shear stress level, the long transient is absent when restarting motion. If, on the contrary, the stop is performed under zero shear stress, the wide bump reappears. This strongly suggests that these transients, associated with the presence of stronger corrugations of the confining substrate potential, are due to gradual stretching and alignment of the constitutive molecules, which persists when the shear stress is maintained, and relaxes otherwise. Such rubbing-induced alignment has been documented already long ago by Pooley and Tabor [97] on teflon, a material for which it is particularly strong. It would be desirable, following these authors, to test this interpretation by devising a set-up which would permit to change the sliding direction by e.g.  $90^\circ$ .

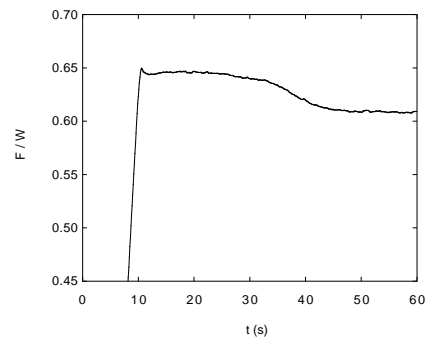


FIG. 33: Reduced friction force versus time after a 300s stop under zero shear stress. The rough PMMA slider is driven at  $V = 10\mu\text{m/s}$  on a poorly silanized track.

This observation naturally raises the question of the *competition between jamming and adhesive pinning to the*

<sup>29</sup> Except possibly for some elastomers under low normal stress and in contact with highly passivated substrates.

<sup>30</sup> When established sliding is not steady, but occurs via stick-slip, static aging results in the growth of the *first* peak with stopping time.

*substrate*. It is reasonable to expect that, the lower the confining pressure  $P$ , the weaker the jamming, i.e. the relative contribution of STZ flips to dissipation.

In boundary lubrication experiments performed in the SFA, pressure levels are smaller than those in MCI junctions by at least two orders of magnitude. As mentioned in §III.C.2, the amplitude of the transients observed on squalane by Drummond and Israelachvili [82] is larger when stopping under smaller shear stress. They also seem to be associated with quite broad stress bumps. This leads one, following the authors, to associate these transients with molecular alignment. Whether or not a narrow glassy-like aging peak is observable at the highest SFA pressures would be worth investigating in detail.

This remark points toward the need for trying to bridge, for given interfacial materials, between SFA and MCI pressure levels, for example with the help of the ball-on-flat configuration. Such comparisons are necessary in order to appreciate to which extent SFA data can be safely extrapolated to the conditions prevailing in macroscopic contacts between hard solids.

The other limiting situation of purely adhesive pinning. It is exemplified by gelatin gels in contact with glass under zero or very small [63] normal load (§III.D). In this case the junction is constituted of a (semi) dilute solution of protein segments in water – no jamming can be invoked. The pinning responsible for the finite static threshold is due to adsorption of the polymer molecules onto the glass substrate, and one may, at least semi-quantitatively, identify the state variable  $\varphi$  with the areal density of adsorption bonds. Such a structure is able to relax by a combination of thermal desorption, chain configuration rearrangements and readorption which leads, at rest, to the slow increase of  $\varphi$ . The number of candidate sites on a segment of course depends on the chemical nature of the network-forming polymer chains. This dynamical problem, although non trivial, might be amenable to a theoretical treatment which would extend equilibrium studies such as those of Subbotin et al. [90] along the lines of the Schallamach-like steady state model built by Charitat and Joanny [88] for the case where only the end monomer is adsorbable.

In such a completely non-jammed junction, frictional dissipation contains two contributions due respectively to :

- Thermally helped advection-induced depinning. It is this mechanism which controls the solid friction behavior proper for such *adsorption-controlled interfaces*.

- Viscous flow of the polymer-water mixture in the sheared interfacial layer.

While the latter is velocity-strengthening, the former decreases with decreasing  $\varphi$ , so it is basically velocity-weakening.

Elastomers probably correspond to an intermediate situation. The interfacial junctions which they form certainly have a dense polymer content, while clearly not

being solid (jammed), since their bulk itself is not. Junction thickness scales as the distance between entanglements. One of the open questions is that of evaluating realistically the viscous contribution to friction of such sheared layers. Whether they exhibit, as might be expected, slow aging at rest is not documented yet, as far as all experiments on elastomer friction have focussed up to now on the steady sliding behavior and on its temperature dependence.

#### IV. CONCLUSION

The route we have chosen to follow in this review has led us from macroscopic dynamics down to gradually decreasing space scales. Solid friction thus appears as a particularly favorable area of material science in which the governing mechanisms are “universal” enough to allow for a rather general phenomenology down to the nanoscopic level.

A first level of analysis, relevant to the widespread case of macroscopic interfaces between rough hard solids, identifies two main physical ingredients :

- (i) A shear-induced depinning process, in which mechanical instabilities lead to structural rearrangements of nanometric shear transformation zones within the junctions where shear localizes. It is the associated multistability of these glassy junctions which is responsible for the existence of finite friction thresholds.

- (ii) Geometric aging, i.e. slow creep growth of the area of the sparse microcontacts forming such interfaces under the high contact pressures associated with this geometry. Sliding limits the duration of contact life, making geometric age a dynamical variable with a memory of the sliding history.

This description provides the physical basis of the Rice-Ruina constitutive laws which, when properly extended, account for all the main features of the low velocity frictional dynamics. It also permits to point more precisely the limits of such a constitutive law. Among these, an important one is concerned with higher velocities — typically  $\gtrsim$  a few  $100\mu\text{m}/\text{sec}$  — at which geometric age becomes small, leading to the saturation of the destabilizing  $V$ -weakening behavior of dynamic friction, and to its inversion into  $V$ -strengthening. Behaviors in the intermediate (mm/sec to cm/sec) range are still insufficiently documented experimentally to allow for detailed models of dissipation in this regime.

For still faster sliding, self-heating becomes non negligible, turning temperature into a new relevant state variable which affects junction rheology. An example of such an effect is that of the stick-slip dynamics of the bowed violin string, which has been modeled by Smith and Woodhouse [98] in terms of the triggering by slip-induced heating of a transition from sticking solid to viscous fluid of the rosin rubbed on the bow.

Beyond the slow dynamics leading to the notion of geometric age, another one emerges, associated with structural aging of the junctions, whose effects are masked, for rough-on-rough systems, by the larger geometric aging ones. Structural aging at rest and its counterpart – rejuvenation when sliding – is at work in all types of frictional junctions, leading to slow growth of static thresholds with time and to stick-slip-like dynamical instabilities. It affects the topography of the multistable energy landscapes which govern frictional rheology. Further experimental information will be needed in order to try and specify it in terms of precise state variables, whose nature is probably not unique.

On the basis of comparisons between different classes of interfaces, we have suggested a schematic classification in terms of two limiting types.

(i) *Jammed junctions*, solidified under confinement into a soft glass structure. They are relevant at high contact pressures such as met with multicontact interfaces. Multistability results from their glassy structure itself, and in this case frictional dissipation enters the wider class of problems constituted of plasticity of amorphous media and soft glass rheology.

(ii) *Purely adhesive junctions* for which pinning is due to adsorption bonds between the junction molecules and the substrates(s). They form at contacts under low confinement pressures involving gels and, more generally, polymers.

Many real junctions probably are a compound of these two ideal types, their frictional dissipation containing contributions of both types whose respective weights depend on pressure, temperature, density and on the physico-chemical nature of the confining surfaces.

While, in our opinion, the question of geometric age effects in multicontact solid friction is now reasonably cleared up, that of junction rheology remains a largely open issue worth of further investigation. In order for modelization to make significant progress, more detailed experimental information is needed, in particular about :

- Systematic trends associated with varying pressure and temperature, for systems with controlled surfaces.
- The effect of various aging histories, paralleling analogous studies in structural and spin glasses. In the case of adsorption-controlled junctions, information about aging might also be obtained via adhesion tests [99], provided that these be performed on materials with negligible viscoelasticity.

Numerical simulations of sheared junctions in the presence of realistic confining potentials should also be of great help.

Finally, the reader may have been surprised that we never used terms such as “nanofriction” or “nanotribology”. This we did purposefully, since we consider them rather misleading. Indeed, “nanotribology” is often associated with investigations of the nature of the basic dissipative processes which, as we saw, occur on the nano-

metric scale. However, friction, as defined in terms of a stress or a friction coefficient, results from the self averaging of such events within contacts of, at least, mesoscopic (micrometric) size. This is precisely why friction laws do not make sense on the nanometric scale.

We consider that the term nanofriction should be reserved for situations where lateral contact sizes are themselves of nanometric order, in which case different effects may emerge, such as exemplified by aging due to capillary condensation [100]. It is also likely that, in such regimes, the nature of dissipative processes [101] is different from that in mesoscopic contacts.

### Acknowledgments

We are particularly grateful to J.R. Rice, K.L. Johnson and Y. Bréchet for encouraging our first steps in the field of friction, and letting us benefit liberally from their vast knowledge of mechanics and material science. We are deeply indebted to P. Nozières, B. Perrin, B. Velicky and F. Heslot for their precious contributions at various stages of our work on this subject, as well as to L. Bureau and O. Ronsin for a long lasting collaboration, and fruitful exchanges on these and related subjects.

### Appendix A : Shear stiffness of a MCI

Already long ago, a number of studies have tried to get independent information about the structure of MCI from the load dependence of various interfacial properties besides friction. These include electrical [11] and thermal [102] conductances, variations of closure with normal load [103], acoustic reflection and interfacial normal and transverse mechanical stiffnesses [104]. In order to confront experimental results with the Greenwood-Williamson model, each of these properties must be calculated within this same frame.

Let us sketch out, as an example, the evaluation of the interfacial shear stiffness. For a single Hertz contact of radius  $a$  between two identical spheres of shear modulus  $G$  and Poisson ratio  $\nu$ , it was calculated by Mindlin [105] [13] to be :

$$k_s = \frac{4Ga}{2 - \nu} \quad (57)$$

which expresses the fact that the strain energy due to shearing is essentially localized, in each medium, within a volume of section  $\sim a^2$  and height  $\sim a$ . So, the relative shear displacement involved in the definition of  $k_s$  is that between any two points on both sides of the contact at distances  $\gg a$  from it.

Consider a set of  $n$  GW microcontacts between two blocks of thickness  $D$ , shear modulus  $G$ . One may separate this elastic system into an interfacial layer of thickness  $\gg a$  but  $\ll D$  sandwiched between two bulk regions

of thickness  $\simeq D$ . As far as  $\Sigma_R \ll \Sigma_{app}$ , the microcontacts are elastically independent, and the total *interfacial stiffness*  $K_s$  is simply the sum of the individual ones, i.e., with the notations of § II.C :

$$K_s = \frac{4G}{2-\nu} n\bar{a} \quad (58)$$

From equations (8), (9)

$$K_s = \frac{4G}{(2-\nu)\sqrt{\pi E}} \frac{W}{s} = \frac{2}{(2-\nu)(1+\nu)} \frac{W}{s} \quad (59)$$

So, the GW model predicts, contrary to immediate intuition, that the interfacial stiffness of an elastic MCI is independent of the bulk material shear modulus.

Of course, experiments measure the compound response of the interface and the bulk. A more important warning comes from the fact that expression (57) is valid only in the limit of very small ratios of shear to normal forces. Indeed, Mindlin has shown [13] that increasing shear induces, at the periphery of the contact, a slipping annulus along which, would it remain non-slipping, the friction sliding threshold would be overcome. This effect results in a non-linear weakening behavior of  $k_s$  [13] and of the MCI response [106].

Consider now a GW interface in the fully plastic limit. When a small shear force is applied for the first time, it induces some further plastic flow, probably leading to some small adaptation of contact radii. Under subsequent unloading-reloading cycles, these adapted contacts respond elastically, with an individual stiffness  $\sim Ga$ .  $K_s$  is then immediately evaluated to be  $\sim W/\lambda$ , where the length  $\lambda$  is of the order of  $s/\psi$ , with  $\psi$  the plasticity index defined in section II.C [17].

The experiments of Berthoud and Baumberger [17] on PMMA (a polymer glass)/PMMA and AU4G (an aluminum alloy)/AU4G have confirmed the Amontons-like behavior (59) of  $K_s$ . The lengths  $\lambda$  for the two systems were different, but both on the order of a few microns. They were found to be compatible, in order of magnitude, with the values predicted from the above model. These results confirm the robustness of the three properties of MCI, listed in section II.C, which emerge from the GW model.

In view of the difficulty of determining accurately  $s$  and, even more,  $R$ , as well as of the numerous approximations involved in the GW model and, even more, of its elasto-plastic extension, it would be fallacious to expect a more quantitative agreement.

Amontons-like behaviors have also been measured to hold, with various degrees of accuracy depending on the specific difficulties inherent to each experimental method, on the other interfacial properties listed at the beginning of this Appendix.

### Appendix B : The viscoelastic GW model

Our derivation summarizes the work of Hui et al [31].

Let us consider a MCI between a linear viscoelastic, incompressible and isotropic medium and a rigid one – a good approximation for contact between a rough elastomer and a rough hard solid. We want to describe this MCI in the the frame of the simplest version of the GW model (exponential distribution of summit heights).

In a linear viscoelastic material, shear stress and strain are related via a retarded elastic shear modulus  $G(t)$ , by the constitutive equation :

$$\sigma(t) = \int_{-\infty}^t dt' G(t-t') \frac{d\epsilon(t')}{dt'} \quad (60)$$

which can be formally inverted into

$$\epsilon(t) = \int_{-\infty}^t dt' J(t-t') \frac{d\sigma(t')}{dt'} \quad (61)$$

$J(t)$ , which characterizes the strain response to a unit stress step applied at  $t = 0$ , increases with time, as a result of the progressive relaxation of the constitutive polymer molecules.

Let us first consider the viscoelastic analogue of the single Hertz contact (§ II.A.2), created by applying the load  $w$  at time  $t = 0$ . It is intuitively clear that, since the compliance increases, the compression  $\delta(t)$  and the contact radius  $a(t)$  increase monotonously. Lee and Radok [107] have shown (see also [13]) that in such a case the solution of the contact problem is that deduced from the Hertz one by simply replacing the shear modulus by its retarded counterpart  $G(t)$ . So, the Hertz load-radius relation (eq. (3)) becomes :

$$w = \int_{-\infty}^t G(t-t') \frac{d}{dt'} \left[ \frac{4}{\pi R^*} a^3(t') \right] \quad (62)$$

with  $a^2(t') = R^* \delta(t')$ .

We now turn to the corresponding GW problem, contact under the normal load  $W$  being first established at  $t = 0$ . As time increases, clearly, the interfacial separation  $d(t)$  will decrease monotonously, the number of microcontacts  $n(t)$  and their individual area increase, leading to the increase of the real area of contact  $\Sigma_r(t)$ .

The three GW equations (eqs.(5) - (7)) become :

$$n(t) = N \int_{d(t)}^{\infty} dz \frac{1}{s} e^{-z/s} \quad (63)$$

$$\Sigma_r(t) = N \int_{d(t)}^{\infty} dz \pi R (z - d(t)) \frac{1}{s} e^{-z/s} \quad (64)$$



$$W(t) = N \int_{d(t)}^{\infty} dz \frac{1}{s} e^{-z/s} \int_{-\infty}^t dt' \theta(t' - t_0(z)) G(t - t') \frac{d}{dt'} \left( \frac{4}{3} R^{1/2} (z - d(t'))^{3/2} \right) \quad (65)$$

where  $\theta$  is the unit step function,  $W(t) = W\theta(t)$ , and the function  $t_0(z)$  is the inverse of  $d(t)$ , i.e.

$$d(t_0(z)) = z \quad (66)$$

Equation (65) is based upon relation (62) and states that each contact with summit height  $z$  existing at time  $t$  has contributed since  $t' = t_0(z)$  when it first appeared, i.e. for  $t' > t_0(z)$  or equivalently,  $d(t') < z$ .

Setting  $y = (z - d(t'))/s$  and performing the  $y$ -integration in eq.(65) yields :

$$W(t) = N (\pi R s^3)^{1/2} \int_{-\infty}^t dt' G(t - t') \frac{d}{dt'} \left( e^{-d(t')/s} \right) \quad (67)$$

which can be inverted, with the help of definitions (60), (61) into :

$$e^{-d(t)/s} = \frac{1}{(\pi R s^3)^{1/2}} \int_{-\infty}^t dt' J(t - t') \frac{dW(t')}{dt'} \quad (68)$$

On the other hand, from equation (64)

$$\Sigma_r(t) = N \pi R e^{-d(t)/s} \quad (69)$$

so that, finally, since  $dW/dt' = \delta(t')$ , the real area of contact evolves according to :

$$\Sigma_r(t) = \sqrt{\frac{\pi R}{s}} J(t) W \quad (70)$$

### Appendix C : The driven block : Linear stability analysis

Consider the system defined in §II.D.2, made of a block of mass  $M$ , carrying the normal load  $W$ , driven at the constant velocity  $V$  through a spring of stiffness  $K$  <sup>31</sup>. The equations describing the motion read :

$$M\ddot{x} = -K(x - Vt - \alpha) - W\mu_d(\phi, \dot{x}) \quad (71)$$

$$\dot{\phi} = 1 - \frac{\dot{x}\phi}{D_0} \quad (72)$$

In the RR model :

$$\mu_d = \mu_{d0} + B \ln \frac{\phi}{\phi_0} + A \ln \frac{\dot{x}}{V_0} \quad (73)$$

with  $V_0$  some reference velocity,  $\phi_0 = D_0/V_0$ . However, in view of the shortcomings of expression (73) discussed in §II.D, we will leave the functional form of  $\mu_d$  unspecified at this stage.

Equations (71), (72) have the stationary solution :

$$x_{st}(t) = Vt - \alpha - \frac{W}{K} \mu_d \left( \frac{D_0}{V}, V \right) \quad (74)$$

$$\phi_{st} = \frac{D_0}{V} \quad (75)$$

In order to study its (linear) stability, we linearize equations (71), (72) in  $\delta x(t) = x(t) - x_{st}(t)$ ;  $\delta\phi(t) = \phi(t) - \phi_0$ . Then :

$$\frac{M}{W} \delta\ddot{x} + \frac{K}{W} \delta x + \frac{\mu_{\dot{x}}}{V} \delta\dot{x} + \frac{V\mu_{\phi}}{D_0} \delta\phi = 0 \quad (76)$$

$$\delta\dot{\phi} + \frac{V}{D_0} \delta\phi + \frac{1}{V} \delta\dot{x} = 0 \quad (77)$$

with  $\mu_{\phi} = \partial\mu_d/\partial(\ln\phi)$ ,  $\mu_{\dot{x}} = \partial\mu_d/\partial(\ln\dot{x})V$ , both quantities being evaluated at  $\phi = D_0/V$ ,  $\dot{x} = V$ . Note that we saw that, for slowly sliding MCI,  $\mu_{\dot{x}} > 0$ ,  $\mu_{\phi} < 0$ , and  $\mu_{\phi} - \mu_{\dot{x}} > 0$ . The solutions of this system are of the form :

$$\begin{pmatrix} \delta x \\ \delta\phi \end{pmatrix} = \begin{pmatrix} \xi \\ \psi \end{pmatrix} e^{i\Omega t} \quad (78)$$

and the frequencies  $\Omega$  of these eigenmodes are the roots of :

<sup>31</sup> We assume that, as is commonly the case,  $K$  is much smaller than the interfacial stiffness. Finite interfacial compliance effects are

evaluated in [50].

$$-i \frac{M}{W} \Omega^3 - \left( \frac{\mu_{\dot{x}}}{V} + \frac{MV}{WD_0} \right) \Omega^2 + \left( \frac{K}{W} + \frac{\mu_{\dot{x}} - \mu_{\phi}}{D_0} \right) i \Omega + \frac{K}{W} \frac{V}{D_0} = 0 \quad (79)$$

If, for all roots,  $Im\Omega > 0$ , all (infinitesimal) fluctuations about the stationary state decay, steady sliding is (locally) stable. For very large  $K$  the solutions of (79) read :

$$\Omega_1 \simeq \frac{iV}{D_0} \quad \Omega_{\pm} = \pm \sqrt{\frac{K}{M}} + (1 + 3i) \frac{W\mu_{\dot{x}}}{MV} \quad (80)$$

Since  $\mu_{\dot{x}} > 0$ , the system is stable in the large  $K$  limit. As the stiffness decreases, it becomes unstable if, and when, the imaginary part of one at least of the roots vanishes. One easily checks on equation (79) that this occurs when :

$$\frac{K}{W} = \left( \frac{K}{W} \right)_c = (\mu_{\phi} - \mu_{\dot{x}}) \left( 1 + \frac{MV^2}{WD_0\mu_{\dot{x}}} \right) \quad (81)$$

As expected, instability only occurs when  $\mu_{\phi} - \mu_{\dot{x}} > 0$ , i.e. (see §II) when the steady sliding  $\mu_d$  is velocity-weakening, which is indeed the case for our systems in the  $V$ -range under consideration.

Note that inertia only comes into play in eq.(81) via the quantity  $\theta = (MV^2/WD_0\mu_{\dot{x}})$ . For a block sliding under its own weight ( $W = Mg$ ), with  $D_0 \gtrsim 1\mu\text{m}$ ,  $\mu_{\dot{x}} \approx 10^{-2}$ ,  $\theta \lesssim 10^{-5} (V_{\mu\text{m}/\text{sec}})^2$  can safely be neglected in our low velocity regime, and the position of the bifurcation line is simply given by :

$$\left( \frac{K}{W} \right)_c = \mu_{\phi} - \mu_{\dot{x}} \quad (82)$$

For the RR model,  $\mu_{\phi} - \mu_{\dot{x}} = B - A$  is a constant,  $(K/W)_c$  is  $V$ -independent.

At the bifurcation, the two (complex conjugate) neutral modes oscillate at the critical frequency :

$$\Omega_c = \frac{V}{D_0} \sqrt{\frac{\mu_{\phi}}{\mu_{\dot{x}}} - 1} \quad (83)$$

That is, the bifurcation is of the Hopf type. A third order perturbation expansion can be performed standardly provided that  $\mu_{\phi}$  and  $\mu_{\dot{x}}$  are not mere constants (see §II). It shows that the stick-slip bifurcation is direct - i.e. that the SS amplitude grows continuously when decreasing e.g.  $K$  below its critical value.

Note finally that, for a velocity-strengthening  $\mu_d$ , ( $\mu_{\phi} - \mu_{\dot{x}} < 0$ ), the system is always stable against *infinitesimal* perturbations. This does not preclude the possibility of a *finite* amplitude instability. Brockley [108] has shown that - in the case where  $\mu_{\phi} = 0$  - when one takes inertia into account, the system does exhibit a strongly hysteretic Hopf bifurcation. As explained in §II, one expects this situation to prevail, for rough-on-rough MCI, at large enough driving velocities ( $V > V_{min}$ ) for which geometric aging becomes inactive. A Brockley-like regime has indeed been observed [109], for a paper/paper interface, in the cm/sec range.

#### Appendix D : The Schallamach model of adsorption-controlled friction

Following Schallamach's seminal article [64], consider an extended interface between a soft slider and a hard flat track covered with adhesive sites which can pin the slider molecules. Represent the slider as a set of  $N_0$  identical and *independent* chains of stiffness  $\kappa$ , potentially forming bonds by adsorption of their end monomer onto the track. Adsorption and subsequent desorption are thermally activated, and, when sliding, desorption is aided by advection. The number  $N$  of bonds is therefore expected to be a function of the sliding velocity  $V$  and of the temperature  $T$ . In steady motion, the elastic force exerted on a given bond increases linearly with time until the bond snaps off and the stored energy is dissipated.

The frictional force thus reads :

$$F = N\kappa V \bar{t} \quad (84)$$

where  $\bar{t}$  is the average lifetime of a bond.

Let  $\tau$  be the average time for which a chain remains depinned before re-adsorbing. The stationary number of bonds is :

$$N = N_0 \frac{\bar{t}}{\bar{t} + \tau} \quad (85)$$

and the friction force

$$F = N_0 \kappa V \tau \frac{(\bar{t}/\tau)^2}{1 + (\bar{t}/\tau)} \quad (86)$$

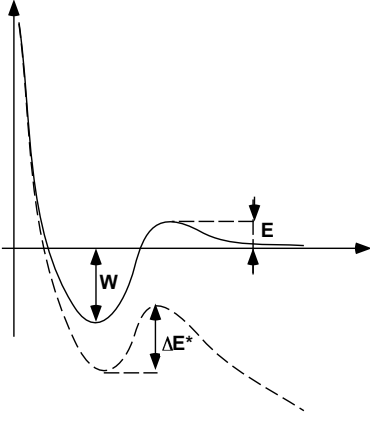


FIG. 34: Sketch of the adhesive pinning potential (full line). When the pinned chain is stretched, the desorption barrier decreases from  $\Delta E = W + E$  to  $\Delta E^*$  (dashed line).

In order to desorb (resp. adsorb), a chain must overcome an energy barrier of height  $\Delta E = W + E$  (resp.  $E$ ), as sketched on Figure 34. When the pinned chain is stretched at velocity  $V$ , the barrier is lowered and its effective height becomes  $\Delta E^* = \Delta E - \kappa b V t$ , where  $b$  is a length of atomic order. Schallamach assumes that the resulting desorption rate is :

$$r(t) = \frac{1}{\tau_0} \exp \left[ -\frac{\Delta E^*(t)}{k_B T} \right] \quad (87)$$

where  $\tau_0^{-1}$  is an attempt frequency, and  $t$  the age of the bond.

Note that this expression for  $r$  tacitly assumes that thermal activation is efficient enough for all bonds to break before reaching the deterministic threshold such that  $\Delta E^* = 0$ , i.e. that  $\Delta E^*(\bar{t}) \gg k_B T$ . We will discuss this assumption in more detail below.

The time  $\tau$  is that for thermal activation above the barrier  $E$ , of unspecified origin, and Schallamach sets :

$$\tau = \tau_0 \exp(E/k_B T) \quad (88)$$

an expression which neglects in particular advection effects.

Consider a set of  $n_0$  bonds all formed at the same time  $t = 0$ . At time  $t$ , the number of these,  $n(t)$ , which have not desorbed obeys :

$$\frac{dn}{dt} = -r(t)n \quad (89)$$

The average bond lifetime  $\bar{t}$  then reads, with the help of equations (87),(89) :

$$\bar{t} = \int_0^\infty \frac{n(t)}{n_0} dt = \tau_{out} \frac{V_0}{V} \int_0^\infty \frac{e^{-y}}{y + (V_0/V)} dy \quad (90)$$

where  $\tau_{out} = \tau_0 \exp(\Delta E/k_B T)$  is the desorption time of the unstretched chain, and  $V_0 = k_B T / \kappa b \tau_{out}$ .

This, together with expression (86), yields the friction force in the steady state. More precisely, in the small and large velocity limits :

$$\bar{t}/\tau_{out} = 1 - \frac{V}{V_0} + \dots \quad (V \ll V_0) \quad (91)$$

$$\bar{t}/\tau_{out} = \frac{V_0}{V} \left[ \ln \frac{V}{V_0} - 0.577 + \dots \right] \quad (V \gg V_0) \quad (92)$$

$\bar{t}$  decreases monotonously with  $V$ , while the elastic energy  $\kappa b V \bar{t}$  stored before debonding increases from linearly ( $V \ll V_0$ ) to logarithmically ( $V \gg V_0$ ) as shown on Figure 35. Also shown on this figure is the average number of bonds in steady state  $N(V)$ , which decreases all the more slowly to zero in the large  $V$  limit that  $\tau/\tau_{out}$  is small.

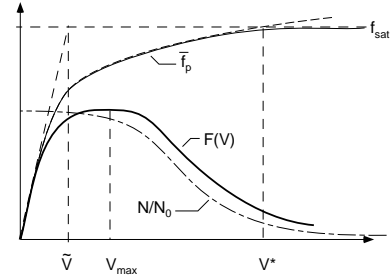


FIG. 35: Qualitative plot of the average pinning force  $\bar{f}_p$  (thin line), the fraction of bonded chains  $N/N_0$  (dashed line), the friction force  $F(V)$  (thick line) as predicted by Schallamach's model, for  $\tau/\tau_{out} \ll 1$ .

As a result  $F(V)$  exhibits a maximum at  $V = V_{max}$  (Figure 35) resulting from the interplay of two effects :

- the decrease with  $V$  of the number of bonds.
- the increase of the average pinning force  $\bar{f}_p = \kappa V \bar{t}$ .

In the limiting regimes :

$$F(V) \simeq N_0 \kappa \frac{\tau_{out}^2}{\tau + \tau_{out}} V \quad (V \ll V_0) \quad (93)$$

$$F(V) \simeq N_0 \frac{\tau_{out}}{\tau} \frac{k_B T}{b} \frac{V_0}{V} \ln^2 \frac{V}{V_0} \quad (V \gg V_{max}) \quad (94)$$

Let us now discuss in more detail Schallamach's results and assumptions. Two weak points in the theory are immediately clear.

- It predicts vanishing friction at large  $V$ , since, in this limit, complete depinning is achieved. The junction is then a mere sheared liquid layer, whose viscous dissipation has been neglected. The corresponding contribution  $F_{vis}(V)$  to the total friction force  $F_{tot}(V) =$

$F(V) + F_{vis}(V)$  becomes dominant for  $V \gg V_{max}$ . Its precise expression of course depends on the nature of the slider material (e.g. hydrogel *vs* elastomer).

- As mentioned above, Schallamach's expression for the desorption rate  $r$  is valid only as long as  $\Delta E^*(\bar{t}) \ll k_B T$ . Since equation (74) results in an unboundedly growing value of  $\kappa b V \bar{t}$  (see Figure 35), this assumption fails for  $V \gtrsim V^*$  such that  $\Delta E = \kappa b V^* \bar{t}(V^*)$ , which yields  $V^* \sim V_0 \exp(\Delta E/k_B T)$ . In this fast regime, we are back to the scenario of § II.C.4. Advection-controlled deterministic bond breaking becomes more efficient than “premature” thermally activated depinning, resulting in a value of  $\bar{f}_p$  which crosses over from the Schallamach logarithmic regime to the deterministic saturation value  $f_{sat} = \Delta E/\kappa b$ . That is, as shown on Figure 35,  $\bar{f}_p$  exhibits three regimes : an initial linear one for  $V \lesssim \tilde{V}$ , a logarithmic one for  $\tilde{V} \lesssim V \lesssim V^*$ , saturation for  $V > V^*$ . The lower crossover  $\tilde{V}$  can be evaluated as  $\tilde{V} \simeq V_0(\Delta E/k_B T) \simeq \Delta E/\kappa b \tau_{out}$ .

Keeping track of these two corrections results in a total friction force curve whose qualitative shape depends on the order of magnitude of the parameter  $\tau/\tau_{out}$ . Note that, within Schallamach's assumption (equation (75))  $\tau/\tau_{out} < 1$ .

If  $\tau/\tau_{out} \ll 1$ , one easily evaluates  $V_{max} \approx V_0 \tau_{out}/\tau$ , so that

$$\frac{V}{V_{max}} \approx \frac{\Delta E}{k_B T} \frac{\tau}{\tau_{out}} \approx \frac{\Delta E}{k_B T} e^{-W/k_B T} \ll 1$$

and  $F(V)$  exhibits a wide plateau followed by a slow decrease. Whether or not the total force  $F_{tot} = F + F_{vis}$  exhibits a  $\mathcal{N}$ -shape for  $V > V_{max}$  depends on the effective viscosity of the unpinned junction and on the density of pinning sites  $N_0$ .

As  $\tau/\tau_{out}$  increases towards 1, the width of the plateau decreases with  $V_{max}$ ,  $F(V)$  becomes steeper on the high- $V$  side, so that the more likely a  $\mathcal{N}$ -shaped  $F_{tot}(V)$ , hence a  $V$ -weakening friction regime leading to stick-slip.

Finally, it is worth recalling that, when the system is loaded from rest at a prescribed velocity  $V_{load}$  larger than, typically,  $\tilde{V}$ , its response is initially quasi-elastic, the upper limit of this regime appearing as a static threshold. Since  $\tilde{V} \sim \Delta E/\kappa b \tau_{out}$ , reasonable estimates lead to conclude that in order for  $\tilde{V}$  to lie in the sub- $\mu\text{m}/\text{sec}$  range, adsorption should be quite strong – corresponding to binding energies  $W$  not far below the eV level.

- 
- [†] “UMR CNRS 7588, Universités Paris 6 et Paris 7”.
- [1] D. Dowson, *History of Tribology* (Longman, New York, 1979).
- [2] T. Baumberger, C. Caroli, O. Ronsin (1999), *Tribology on the 300th anniversary of Amontons' law*, p. 51, M.D. Drory and M.O. Robbins ed. (M.R.S. Warrendale, Penn. USA, 1999).
- [3] B.N.J. Persson, *Sliding friction* (Nanoscience and Technology Series, Springer, Heidelberg, 1998).
- [4] C.H. Scholz, *The Mechanics of Earthquakes and Faulting* (Cambridge University Press, Cambridge, 1990).
- [5] J.H. Dieterich J. Geophys. Res. **84**, 2161 (1979).
- [6] J.R. Rice, A.L. Ruina, J. Appl. Mech. **50**,343 (1983).
- [7] M.L. Falk, J.S. Langer, Phys. Rev E **57**, 7192 (1998)
- [8] *Jamming and Rheology: Constrained Dynamics on Microscopic and Macroscopic Scales* (eds A. Liu and S. R. Nagel) (Taylor and Francis, London, 2001).
- [9] F. Heslot, T. Baumberger, B. Perrin, B. Caroli and C. Caroli, Phys. Rev. E, **49**, 4973 (1994).
- [10] A. Cochard, J.R. Rice, J. Geophys. Res. **105**, 25891 (2000).
- [11] F.P. Bowden and D. Tabor, *The Friction and Lubrication of Solids I* (Clarendon press, London, 1950).
- [12] J.H. Dieterich and B.D. Kilgore, Pure Appl. Geophys. **143**, 283 (1994).
- [13] K.L. Johnson, *Contact Mechanics* (Cambridge University Press, Cambridge, 1985).
- [14] D. Tabor, *The Hardness of Metals* (Clarendon, Oxford, 1951)
- [15] J.A. Greenwood and J.P.B. Williamson, Proc. Roy. Soc. Lond. A **295**, 300 (1966).
- [16] P.R. Nayak, Wear **26**, 165 (1973).
- [17] P. Berthoud, T. Baumberger, Proc. R. Soc. Lond. A **454**, 1615 (1997)
- [18] S.R. Brown, C.H. Scholz, J. Geophys. Res. B **91**, 4939 (1986).
- [19] E. Bouchaud, J. Phys. C **9**, 4319 (1997).
- [20] B.N.J. Persson, J. Chem. Phys. **115**, 3840 (2001).
- [21] B.N.J. Persson, O. Albohr, C. Creton, V. Peveri, J. Chem. Phys. **120**, 8779 (2004).
- [22] M.H. Muser, L. Wenning, G. He, and M.O. Robbins, *Tribology on the 300th anniversary of Amontons' law*, p. 67, M.D. Drory and M.O. Robbins ed. (M.R.S. Warrendale, Penn. USA, 1999).
- [23] S.J. Dokos, J. Appl. Mech. **13**, 148 (1946).
- [24] C. Marone, Ann. Rev. Earth Plan. Sci. **26**, 643 (1998)
- [25] P. Berthoud, T. Baumberger, C. G'sell, and J.-M. Hiver, Phys. Rev. B **59**, 14313 (1999).
- [26] T. Baumberger (unpublished)
- [27] J.H. Dieterich, J. Geophys. Res **77**, 3691 (1972).
- [28] Y. Bréchet, and Y. Estrin, Scripta Met. Mat. **30**, 1449 (1994).
- [29] T. Baumberger, P. Berthoud, and C. Caroli, Phys. Rev. B **60**, 3928 (1999).
- [30] O. Ronsin, K.L. Coeyrehourcq, Proc. R. Soc. Lond. A **457** 1277 (2001).
- [31] C. Y. Hui, Y.Y. Lin, and J.M. Barney, J. Polym. Sci., Part B : Polym. Phys. **38**, 1485 (2000).
- [32] L. Bureau and T. Baumberger (unpublished).
- [33] E. Rabinowicz, J. Appl. Phys., **27**, 131 (1956).
- [34] J.H. Dieterich, Pageoph **116**, 790 (1978)
- [35] M.L. Blanpied, D.A. Lockner, and J.D. Byerlee, J. Geo-

- phys. Res. **100**, 13045 (1995).
- [36] M. Nakatani, J. Geophys. Res. **106**, 13347 (2001).
- [37] M. Brillouin, *Notice sur les Travaux Scientifiques* (Gauthier-Villars, Paris, 1904).
- [38] See for example : D.S. Fisher, Phys. Reports, **301**, 113 (1998).
- [39] C. Caroli, P. Nozières, *Physics of Sliding Friction*, B.N.F.J. Persson and E. Tosatti ed., NATO ASI Series, Series E : Applied Sciences, Vol. 311 (Kluwer, Dordrecht, 1996).
- [40] C. Caroli, P. Nozières, Eur. Phys J. B **4**, 233 (1998).
- [41] L. Bureau, T. Baumberger, and C. Caroli, Phys Rev. E **64**, 031502 (2001).
- [42] S. Sills and R.M. Overney, Phys. Rev. Lett. **91**, 095501 (2003).
- [43] A.S. Argon, V.V. Bulatov, P.H. Mott, U.W. Sutter, J. Rheol. **39**, 37,(1995)
- [44] M.L. Falk and J.S. Langer, Phys. Rev. E **57**, 7192 (1998)
- [45] D.L. Malandro and D.J. Lacks, J. Chem. Phys. **110**, 4593 (1999).
- [46] J.D. Eshelby, Proc. R. Soc. London, Ser. A **241**, 376 (1957).
- [47] G. Picard, A. Ajdari, F. Lequeux, L. Bocquet, Eur. Phys. J. E **15** 371 (2004).
- [48] P. Sollich, Phys. Rev. E **58**, 738 (1998).
- [49] T. Baumberger, C. Caroli, B. Perrin and O. Ronsin, Phys. Rev. E **51**, 4005 (1995).
- [50] A. Cochard, L. Bureau, T. Baumberger, J. Appl. Mech. **70**, 161 (2003).
- [51] K. Ranjith and J.R. Rice, J. Mech. Phys. Solids **47**, 341 (1999).
- [52] T. Baumberger and L. Gauthier, J. Phys. I France **6** 1021 (1996).
- [53] L. Bureau, T. Baumberger, C.Caroli, Phys. Rev. E **62**, 6810 (2000).
- [54] K. Ranjith and J.R. Rice, J. Mech. Phys. Solids **49**, 1207 (2001).
- [55] F.M.F. Simoes, J.A.C. Martins, Int. J. Eng. Sci. **36**, 1265 (1998).
- [56] J.M. Carlson, J.S. Langer, B.E. Shaw, Rev. Mod. Phys. **66**, 657 (1994).
- [57] J.R. Rice, J. Geophys. Res. **98**, 9885 (1993).
- [58] L. Bureau, T. Baumberger, and C. Caroli, Eur. Phys. J. E **8** (2002).
- [59] D. Tabor and R.H.S. Winterton, Proc. R. Soc. London A **312**, 435 (1969).
- [60] J.N. Israelachvili and D. Tabor, Proc. R. Soc. London A **331**, 19 (1972).
- [61] J. Israelachvili, Surf. Sci. Rep. **14**, 109 (1992).
- [62] J.P. Gong, Y. Osada, Progr. Polym. Sci. **27**,3 (2002).
- [63] T. Baumberger, C. Caroli, O. Ronsin, Eur. Phys. J. E **11**, 85 (2003).
- [64] A. Schallamach, Wear **6**, 375 (1963).
- [65] M. Barquins and R. Courtel, Wear **32**, 133 (1975).
- [66] K. Vorvolakos and M.K. Chaudhury, Langmuir **19**, 6778 (2003).
- [67] C. Derec, PhD Thesis, Universite Paris VII (2001).
- [68] B. Abou, D. Bonn, J. Meunier, Phys. Rev. E **64**, 021510 (2001).
- [69] M. Cloitre, R. Borrega, L. Leibler, Phys. Rev. Lett. **85**, 4819 (2000).
- [70] S.M. Fielding, P. Sollich and M.E. Cates, J. Rheol. **44**, 323 (2000).
- [71] C. Derec, A. Ajdari, F. Lequeux, Eur. Phys. J. **4**, 355 (2001).
- [72] V. Viasnoff, F. Lequeux, Phys. Rev. Lett. **89**, 065701 (2002).
- [73] J.N. Israelachvili, P.M. McGuiggan, A.J. Homola, Science **240**, 189 (1988).
- [74] H. Yoshizawa and J. Israelachvili, J. Phys. Chem. **97**, 11300 (1993).
- [75] J. Van Alsten and S. Granick, Langmuir **6**, 876 (1990).
- [76] P.A. Thompson, G.S. Grest, M.O. Robbins, Phys. Rev. Lett **68**, 3448 (1992).
- [77] J. Klein and E. Kumacheva, Science **269**, 816 (1995).
- [78] C. Drummond and J. Israelachvili, Macromol. **33**, 4910 (2000).
- [79] D. Gourdon and J. Israelachvili, Phys. Rev. E **68**, 021602 (2003).
- [80] S. Yamada, G. Nakamura, T. Amiya, Langmuir **17**, 1693 (2001).
- [81] G. Reiter, L.Demirel, J. Peanasky, L. Cai, S. Granick, Tribology Lett. **1**, 1 (1995).
- [82] C. Drummond and J. Israelachvili, Phys. Rev. E **63**, 041506 (2001).
- [83] T. Baumberger, C. Caroli and O. Ronsin, Phys. Rev. Lett. **88**, 75502 (2002).
- [84] D.L. Johnson, J. Chem. Phys. **77**, 1531 (1982).
- [85] T. Tanaka, L.O. Hocker, and G.B. Benedek, Phys. Rev. **59**, 5151 (1973).
- [86] S.M. Rubinstein, G. Cohen, J. Fineberg, Nature **430**, 1005 (2004).
- [87] R.B. Bird, R.C. Armstrong, O. Hassager, *Dynamics of Polymeric Liquids : Fluid Mechanics*, Vol. **1**, 2nd edition (Wiley, New York, 1987).
- [88] T. Charitat and J.F Joanny, Eur. Phys. J. E **3**,369 (2000).
- [89] Yu.B. Chernyak, A.I. Leonov, Wear **108**, 105 (1986).
- [90] A. Subbotin, A. Semenov, M. Doi, Phys. Rev. E **56**, 623 (1997).
- [91] A.D. Roberts, Tribology International (April 1976), p. 75.
- [92] A.R. Savkoor, *Dry Adhesive Friction of Elastomers* Dissertation, Delft University of Technology (1987).
- [93] J.D. Ferry, *Viscoelastic Properties of Polymers* 2nd edition (Wiley, New York, 1970).
- [94] K.A. Grosch, Proc. Roy. Soc. Lond. A**274**, 21 (1963).
- [95] K.C. Ludema, D. Tabor, Wear **9**, 329 (1966).
- [96] A. Schallamach, Wear **17**, 301 (1971).
- [97] C. M. Pooley and D. Tabor, Proc. R. Soc. London A **329**, 251 (1972).
- [98] J.H. Smith, J. Woodhouse, J. Mech Phys. Sol. **48**, 1633 (2000).
- [99] E. Girard-Reydet, R. Oslanec, P. Whitten and H.R. Brown, Langmuir **20**, 708 (2004).
- [100] E. Riedo, F. Lévy and H. Brune, Phys. Rev. Lett. **88**, 185505 (2002).
- [101] K.S. Kim, *Tribology on the 300th anniversary of Amon-ton's' law*, p. 19, M.D. Drory and M.O. Robbins ed. (M.R.S. Warrendale, Penn. USA, 1999).
- [102] F. Boeschoten and E. F. M. Van der Held, Physica **23**, 37 (1957).
- [103] S. R. Brown, C.H. Scholz, J. Geophys. Res. B**90**, 5531 (1985).
- [104] B. W. Drinkwater, R. S. Dwyer-Joyce, P. Cawley, Proc. R. Soc. Lond. A**452**, 2613 (1996).
- [105] R.D. Mindlin, J. Appl. Mech. **16**, 259 (1949).
- [106] L. Bureau, C. Caroli, and T. Baumberger, Proc. R. Soc.

- Lond.A **459**, 2787 (2003).
- [107] E.H. Lee, and J.R.M. Radok, *J. Appl. Mech.* **27**, 438 (1960).
- [108] C.A. Brockley, R. Cameron and A.F. Potter, *J. Lubr. Tech.*, *Trans. ASME* **89**, 101 (1967).
- [109] T. Baumberger, *Physics of Sliding Friction*, B.N.F.J. Persson and E. Tosatti ed., NATO ASI Series, Series E : Applied Sciences, Vol. 311 (Kluwer, Dordrecht, 1996).